

Two decades of improved wetland carbon sequestration in northern mid-to-high latitudes are offset by tropical and southern declines

Received: 24 August 2024

Accepted: 24 June 2025

Published online: 22 July 2025

 Check for updates

Junjie Li^{1,2}, Junji Yuan¹✉, Philippe Ciais¹, Hojeong Kang¹,
Chris Freeman¹, Yuanyuan Huang¹, Yanhong Dong^{1,2}, Deyan Liu^{1,7}, Ye Li^{1,2} &
Weixin Ding¹✉

Terrestrial carbon (C) sink has long been recognized as trending upwards, yet its recent slowdown raises concerns about accelerating climate change. Variations in wetland C sequestration are hypothesized to play a key role in this shift. Here we mapped annual water levels in global wetlands from 2000 to 2020 using 2,295 field-based measurements and predicted the spatiotemporal pattern of wetland net ecosystem production (NEP) in conjunction with other environmental factors. By compiling 934 in situ observations, we estimated a global mean wetland NEP of 56.4 (44.0–68.8) gC m⁻² yr⁻¹. Integrating the NEP dataset with environmental datasets and machine-learning models, we estimated the mean annual global wetland C sequestration between 2000 and 2020 to be 1,004 (961–1,047) TgC, 70% of which originated from tropical wetlands. We observed a decline in global wetland C sinks until 2005, followed by an increase thereafter. Overall, wetland C sequestration was roughly stable during 2000–2020, as gains in northern mid-to-high latitudes were fully overwhelmed by declines in the tropics and southern mid-to-high latitudes. Our findings highlight hydrological change as a dominant driver of increasing regional variability in wetland C sinks, while intensifying hydrological extremes under climate change may undermine the resilience of wetland C sinks and the ecosystem services they support.

Carbon dioxide (CO₂) exerts a disproportionate role in regulating the global carbon (C) cycle and represents the most important greenhouse gas influencing global warming^{1,2}. Alarmingly, atmospheric CO₂ concentrations have increased from 284.7 ppm in 1850 to 419.3 ppm in 2023 (ref. 3), largely due to anthropogenic emissions^{4,5}. Over the same historical period, the land CO₂ sink increased in pace with anthropogenic emissions⁶, driven primarily by CO₂ fertilization, nitrogen inputs and climate warming in northern regions^{7–11}. During 1850–2023, land ecosystems cumulatively sequestered 225 GtC, offsetting ~32% of total anthropogenic

CO₂ emissions⁶. However, a decline in the efficiency of terrestrial C sinks has emerged in the early twenty-first century, probably constrained by limitations in nutrients, water and heat, among other factors^{7,12,13}. The rate of increase in land CO₂ uptake has slowed from 0.045 GtC yr⁻² during 1960–2000 to 0.02 GtC yr⁻² in 2001–2022 (ref. 12). Yet, it remains unclear which land ecosystems (for example, wetlands or forests) or mechanisms are primarily responsible for this recent slowdown.

Wetlands cover 3–13% of the Earth's land surface¹⁴, yet their C storage approaches 520–710 PgC, representing 20–30% or more of the

A full list of affiliations appears at the end of the paper. ✉ e-mail: jjyuan@issas.ac.cn; wxding@issas.ac.cn

global soil C stocks^{15,16}. This substantial pool means that the destabilization of wetland C could pose a major climate risk by turning these ecosystems into net sources of atmospheric CO₂ (ref. 17). However, wetlands can remain the most cost-effective and efficient ecosystems for CO₂ removal when waterlogged conditions are maintained^{18–20}. Despite this, wetlands are not explicitly incorporated into the models used to constrain the global C budget. Accurate assessments of spatiotemporal patterns in global wetland C sequestration will help to reduce uncertainties and better attribute the terrestrial C sink.

Multiple global change factors, for example, CO₂ fertilization, nitrogen deposition, climate warming and shifts in precipitation patterns, have the potential to reshape wetland C sinks^{21–24}. Of these, wetland C dynamics are especially sensitive to changes in hydrological status^{25–27}. Since 1950, 4.85 Mkm² of global wetlands have been lost due to human activities (for example, drainage) and climatic drying²⁵, both of which commonly result in lowered water levels (WLs). Declines in water tables expose C-rich soils to oxygen, accelerating microbial decomposition and ultimately boosting ecosystem respiration (ER)^{28–30}. However, due to the high spatial heterogeneity of wetlands³¹, decomposition rate changes in response to water-table drawdown vary among studies. For instance, several studies report reduced or unchanged decomposition rates under lowered WLs³². Similarly, the response of gross primary production (GPP) to WL decline is not uniform across diverse wetland categories and geographies^{27,33,34}. Considering that GPP and ER are highly uncertain, it remains unclear to what extent and how water-table drawdown directly regulates variations in net ecosystem production (NEP). Lowered WLs may also alter groundwater-dissolved C export³⁵, but global estimates of this pathway are lacking. By contrast, methane (CH₄) emissions generally declined with lowering WLs^{25–27}. However, with highly uncertain NEP and lateral C loss, the impact of lowered WLs on wetland C sinks is still highly variable. Moreover, global patterns in wetland WLs have remained unclear, despite a previous study presenting a static map of terrestrial groundwater table depth based on field observations and a groundwater model³⁶. Addressing the knowledge gap in spatiotemporal patterns of global wetland WLs and their effects on wetland C fluxes (for example, CO₂ and CH₄ fluxes) is critical for resolving the role of wetlands in the terrestrial C sink under changing hydrologic regimes.

Here, by compiling 2,295 *in situ* measurements from 606 published papers and developing machine-learning models (Extended Data Fig. 1), we mapped wetland WLs at 0.25° × 0.25° resolution (Extended Data Fig. 2) and investigated the spatiotemporal pattern of annual mean WLs of global wetlands. The WL dataset was then used to predict spatial and temporal variations in wetland NEP. Furthermore, a global dataset containing 934 site–year records of field observations of NEP for wetlands was extracted from 258 peer-reviewed publications and the FLUXNET database (Fig. 1a). Of these, 729 and 205 site–year records were measured using the eddy covariance method and the chamber method, respectively. Previous studies proposed that NEP from peer-reviewed papers based on these two methods are of equivalent accuracy, despite potential differences in precision^{25,37}. NEP is the difference between GPP and ER (GPP – ER), with positive values representing net CO₂ uptake and vice versa. Note here that our estimates of wetland C sinks may be overestimated because of the exclusion of CH₄ emissions and groundwater-dissolved C losses^{38,39}. Based on the compiled global dataset, we built a data-driven upscaling approach that models spatial and temporal variations in wetland NEP from hydrology, climate, soil, vegetation and topography. To prescribe wetland extent, we used three data products (Supplementary Fig. 1): WAD2M v.2.0 (13.6 Mkm²), derived from multisensor remote sensing⁴⁰; GLWD v.2.0 (10.8 Mkm²), compiled from a selection of maps and charts³¹; and GIEMS-MC (11.2 Mkm²), generated by integrating GIEMS v.2.0 and GLWD v.2.0 (refs. 41,42). By combining the global gridded NEP estimates with these wetland extent datasets, we evaluated the spatiotemporal pattern of global wetland C sequestration during 2000–2020.

Results and discussion

Characteristics of global wetland NEP

Our global-scale *in situ* database indicated that wetland NEP was usually positive for most observations, with a mean uptake of 56.4 (95% confidence interval (CI) 44.0 to 68.8) gC m⁻² yr⁻¹, indicating that wetlands predominantly function as a net C sink (Fig. 1b). This global mean was approximately 1.5–3.0 times lower than the arithmetic mean values reported by Lu et al.⁴³ and Mitsch et al.¹⁹ (Fig. 1c), largely due to differences in data coverage and representativeness⁴⁴. Lu et al.⁴³ compiled NEP data from 22 freshwater wetlands and derived a mean annual NEP of 93.15 gC m⁻² yr⁻¹, while Mitsch et al.¹⁹ estimated a substantially higher global mean of 186.06 gC m⁻² yr⁻¹ based on data from 21 sites. Both of these earlier studies were based on relatively small sample sizes and were heavily weighted towards marshes, which tend to exhibit higher NEP due to elevated plant primary productivity^{45,46}. Our NEP dataset incorporates 222 wetland sites distributed globally that encompass various climate zones and wetland types and therefore provides a more representative basis for estimating global wetland NEP. Recently, Li et al.¹⁸ estimated a mean NEP of 43.0 gC m⁻² yr⁻¹ for global inland wetlands and peatlands, 24% lower than our estimates. However, their dataset encompassed inland open waters (for example, lakes, rivers, reservoirs and so on) and human-influenced wetlands (for example, rice paddies, drained wetlands and so on), which are beyond the scope of our study. These systems generally exhibit low CO₂ sequestration capacity and can even act as sources of CO₂ (refs. 25,26,47–50).

In terms of climate zones, the average NEP was 89.4 (95% CI 17.1 to 161.7) gC m⁻² yr⁻¹ for tropical wetlands, 79.7 (95% CI 56.7 to 102.8) gC m⁻² yr⁻¹ for temperate wetlands, 39.9 (95% CI 26.5 to 53.2) gC m⁻² yr⁻¹ for boreal wetlands and 21.7 (95% CI 11.7 to 31.7) gC m⁻² yr⁻¹ for Arctic wetlands (Fig. 1d). This latitudinal gradient probably reflects the influence of warmer climates, longer growing seasons and higher availability of diffuse light in tropical and temperate regions, all of which enhanced C sequestration^{7,51–53}. Furthermore, our dataset revealed that WLs were generally higher in tropical and temperate wetlands (Extended Data Fig. 1b), further contributing to stronger C sinks relative to boreal and Arctic wetlands¹⁸. Among wetland types, the highest NEPs were observed in marshes (168.1 gC m⁻² yr⁻¹ with a 95% CI of 126.3 to 209.9 gC m⁻² yr⁻¹) and swamps (150.4 gC m⁻² yr⁻¹ with a 95% CI of 63.8 to 237.0 gC m⁻² yr⁻¹), both significantly higher than the values in peatlands, that is, bogs, fens and peat swamps (Fig. 1e). Specifically, NEP was estimated at 32.8 (95% CI 20.1 to 45.6) gC m⁻² yr⁻¹ for bogs, 38.2 (95% CI 21.5 to 54.9) gC m⁻² yr⁻¹ for fens and –65.8 (95% CI –198.2 to 66.6) gC m⁻² yr⁻¹ for peat swamps. The relatively high NEPs in marshes and swamps are attributed to their high primary productivity^{43,45,46,54} and higher WLs (Extended Data Fig. 1c), which together foster strong C sequestration. For peatlands, flooded conditions are not the typical hydrological and biogeochemical condition²⁶, which aligns with our findings that WLs in bogs, fens and peat swamps are markedly lower than the ground surface. Given this, C-rich upper soil layers in peatlands have more risk to be exposed to oxygen, thus accelerating peat decomposition and CO₂ emissions, which can offset CO₂ uptake by plant photosynthesis^{25–27,55}. Peatlands (peat swamps in particular) are therefore vulnerable to becoming net C sources^{56,57}. Moreover, NEPs in seasonal or permanent inundated floodplains (26.1 gC m⁻² yr⁻¹ with a 95% CI of –12.2 to 64.4 gC m⁻² yr⁻¹) and wet tundras (2.0 gC m⁻² yr⁻¹ with a 95% CI of –10.7 to 14.7 gC m⁻² yr⁻¹) were significantly lower than in marshes and swamps, but not significantly different from peatlands.

Key factors controlling wetland NEP

Based on random forest (RF) analysis, we calculated the relative importance of each predictor variable, including WL, mean annual air temperature (MAT), mean annual precipitation (MAP), photosynthetically active radiation (PAR), evapotranspiration (ET), normalized difference vegetation index (NDVI), enhanced vegetation index (EVI), soil organic carbon (SOC), pH, bulk density (BD), clay content (Clay), sand

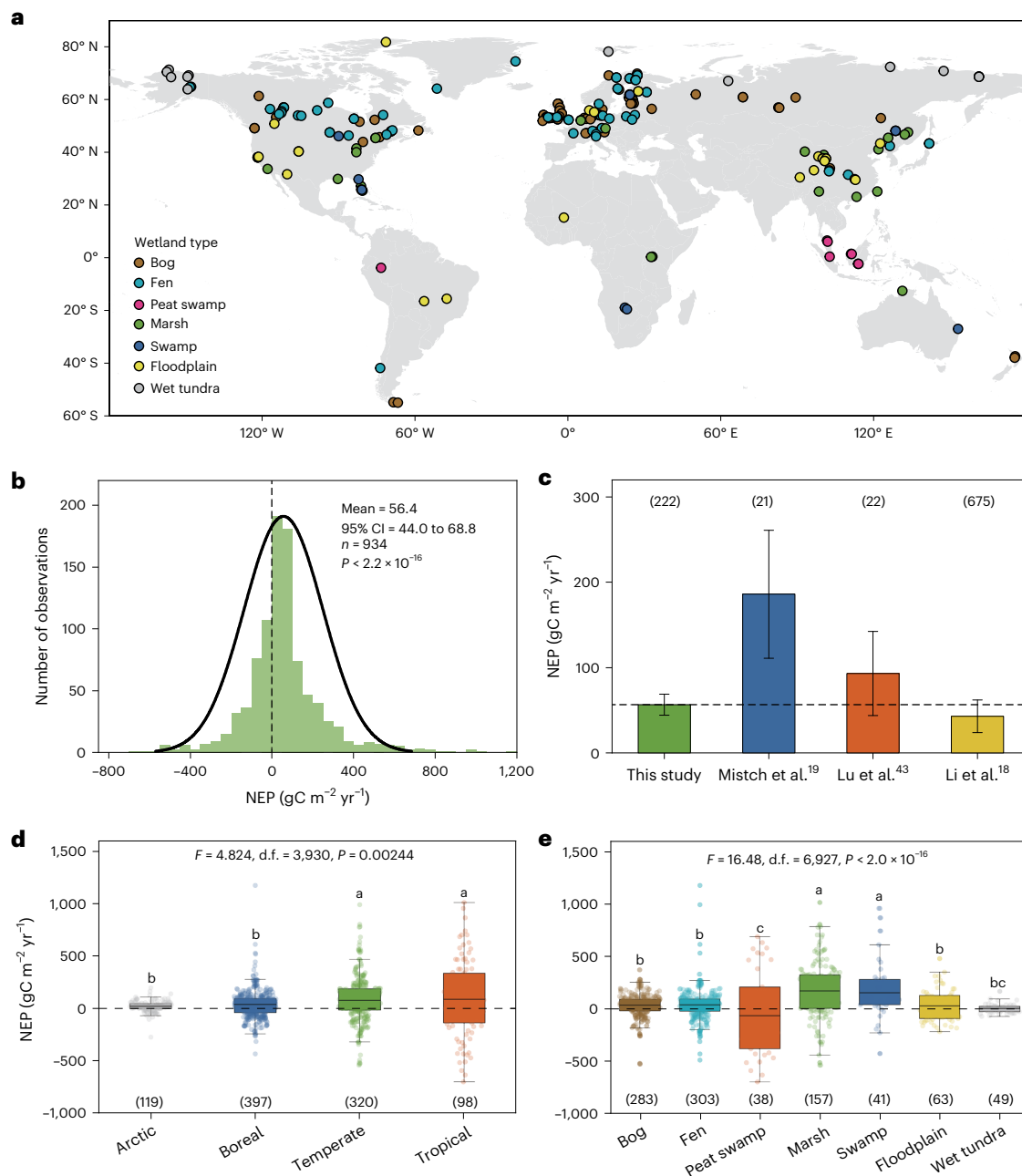


Fig. 1 | Characteristics of global wetland NEP. **a**, The global distribution of field observations of wetland NEP included in our compiled dataset. The wetland types are shown as coloured dots. **b**, Histogram plots exhibiting the annual wetland NEP at the global scale. n represents the sample size. The P value means the statistical significance between annual NEP and zero, as determined by using a two-sided, one-sample t -test. **c**, A comparison of global mean annual wetland NEP synthesis from this study with Mitsch et al.¹⁹, Lu et al.⁴³ and Li et al.¹⁸. The error bars represent the 95% CI. The numbers of wetland sites included in synthesis studies are shown in parentheses. The horizontal dashed black line represents the global mean annual wetland NEP derived from this study. **d,e**, Box plots of

annual wetland NEP in different climate zones (**d**) and wetland types (**e**). Note here that the definition of floodplain denotes seasonal or permanent inundated floodplain. For each box plot, individual data points are shown as coloured dots. Centre lines inside the boxes represent means. Box boundaries represent the 75th and 25th quantiles, and whisker caps represent the 95th and 5th quantiles. Different lowercase letters indicate significant differences at $\alpha = 0.05$, as determined by using one-way analysis of variance (ANOVA) and least significant difference (LSD) tests. No adjustments were made for multiple comparisons. Numbers in parentheses next to the x axis indicate sample sizes (n). F, variance ratio; d.f., degrees of freedom.

content (Sand), silt content (Silt), cation exchange capacity (CEC), base saturation (BS) and elevation. Consistent with previous studies^{18,25–27}, our findings confirmed that WLs exerted the strongest influence on wetland NEP when compared with other biotic and abiotic predictor variables (Fig. 2a). Here, a positive WL value indicates inundation above the ground surface and vice versa. Responses of NEP to WLs were nonlinear and detected by the partial dependence plot from the RF

model⁵⁸. When WLs ranged from -30 to +75 cm, wetland NEP across the globe and extratropical regions was highly sensitive to WLs and decreased with declining WLs (Extended Data Fig. 3). Outside this range, NEP was relatively stable. In tropical wetlands, NEP exhibited a sharp reduction as WLs decreased from +15 to -30 cm, but was largely unresponsive when WLs fell below -30 cm or rose above +15 cm. To validate these patterns, we further analysed the subset database of sites with

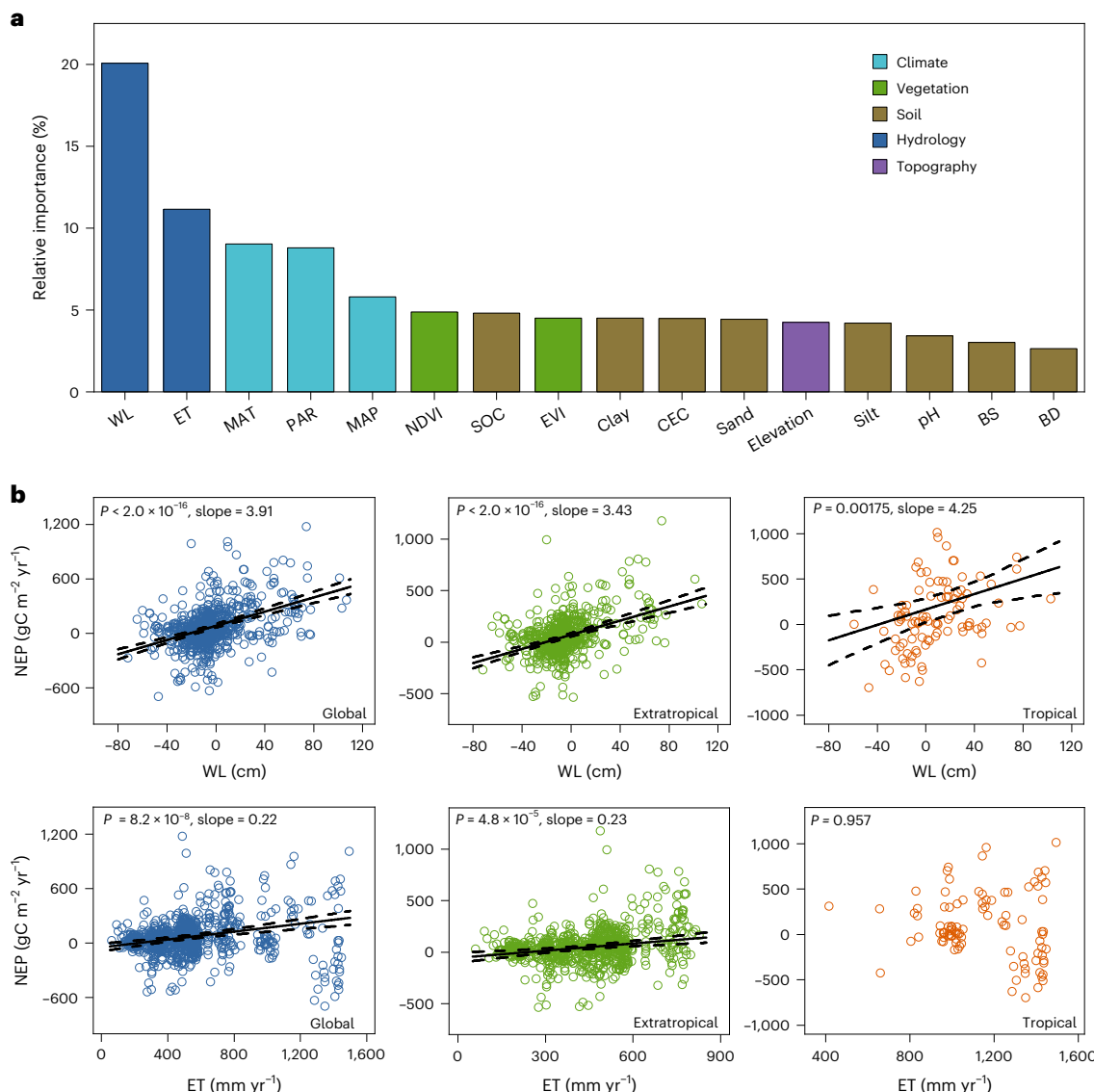


Fig. 2 | Key factors controlling wetland NEP at the global scale. **a**, The relative importance (%) of variables for predicting annual wetland NEP identified by the RF model. **b**, Linear relationships of annual NEP with WL and ET for global wetlands and wetlands in extratropical and tropical regions. Solid and dashed

black lines represent average predicted values and the corresponding 95% CI, respectively, according to linear mixed-effect modelling. Statistical tests are conducted as two sided.

concurrent NEP and WL measurements and found consistent nonlinear relationships (Supplementary Fig. 2). Furthermore, we applied the linear mixed-effect model to determine the overall average sensitivity of NEP to WLs and then assessed the variation in sensitivity among climate zones and studies⁵⁹. The overall average sensitivity of NEP to changes in WLs was $3.91 \text{ gC m}^{-2} \text{yr}^{-1} \text{cm}^{-1}$ ($P < 2.0 \times 10^{-16}$) (Fig. 2b), aligning with a previous estimate of $4.27 \text{ gC m}^{-2} \text{yr}^{-1} \text{cm}^{-1}$ by Zou et al.²⁵ (Extended Data Fig. 4). However, Evans et al.²⁶ and Li et al.¹⁸ reported stronger responses of wetland NEP to WL variations, probably due to their inclusion of human-perturbed wetlands, which tend to exhibit stronger hydrological responses. In addition, we found that NEP sensitivity to WLs was greater in tropical wetlands ($4.25 \text{ gC m}^{-2} \text{yr}^{-1} \text{cm}^{-1}$; $P = 0.00175$) than in extratropical regions ($3.43 \text{ gC m}^{-2} \text{yr}^{-1} \text{cm}^{-1}$; $P < 2.0 \times 10^{-16}$), underscoring the heightened vulnerability of tropical wetlands to hydrological variability.

Following WL, ET emerged as the second most important determinant of wetland NEP. In extratropical wetlands, ET was positively correlated with NEP ($P = 4.8 \times 10^{-5}$), while no significant relationship was found in tropical wetlands. This linkage is probably mediated by WL, as ET can influence the water availability and hydrology of wetlands

(Extended Data Fig. 5). Moreover, enhanced stomatal CO₂ uptake during photosynthesis is generally accompanied by higher water loss through transpiration^{60,61}, further reinforcing the positive relationship between ET and NEP. MAT also exhibited a positive correlation with NEP in extratropical wetlands ($P = 0.0039$) but had negligible effects in tropical wetlands (Extended Data Fig. 6). Warmer climate tends to promote plant growth and extend growing seasons^{7,62–64}, thereby improving C sequestration capacity in extratropical wetlands. PAR likewise linearly increased wetland NEP within the extratropical zone ($P = 0.000964$) but showed no effect on wetland NEP in the tropics. PAR is the portion of the light spectrum utilized by plants for photosynthesis⁶⁵. Accelerated net CO₂ uptake can be achieved with high PAR and the accompanying enhanced plant photosynthesis^{7,53}.

Spatiotemporal patterns in global wetland C sequestration

To extend our findings beyond the 934 site-year observations of wetland NEP, we built global wetland NEP maps at $0.25^\circ \times 0.25^\circ$ resolution using the RF algorithm (Fig. 3a). The RF model outperformed two alternative machine-learning algorithms, that is, extreme gradient

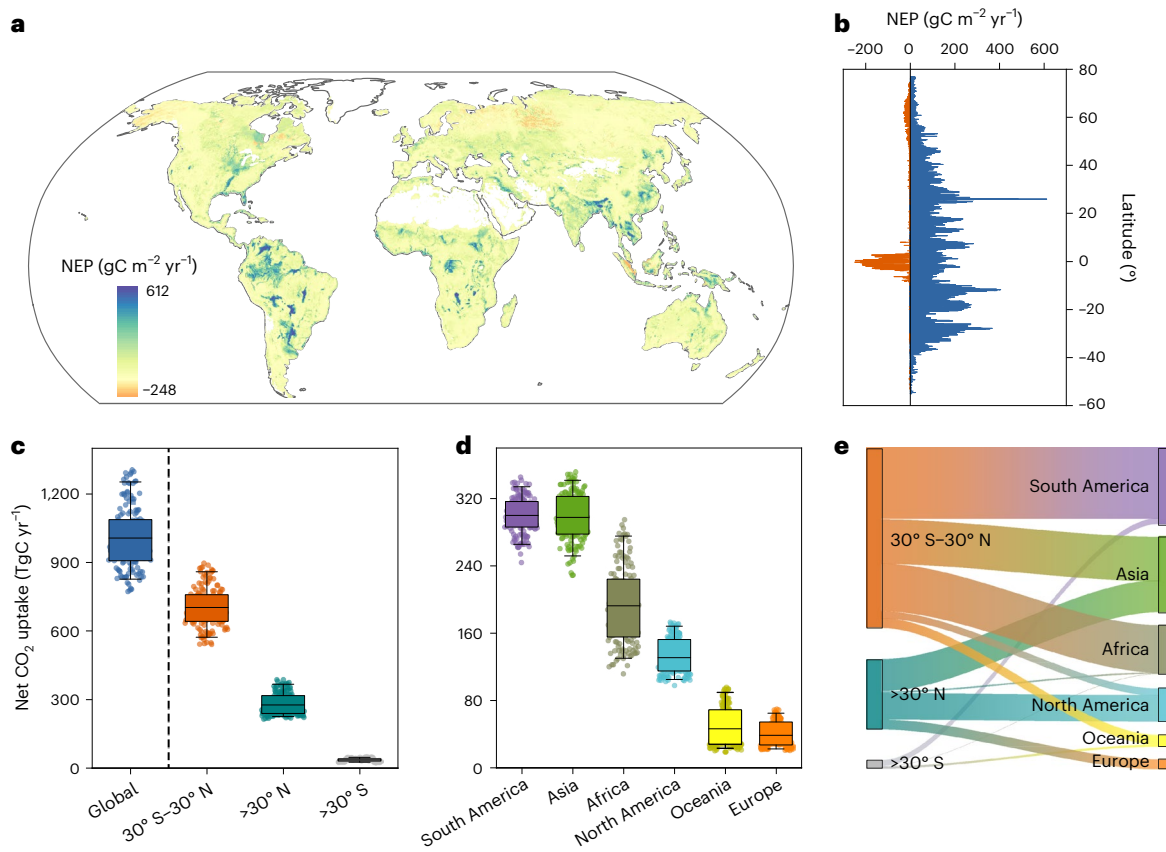


Fig. 3 | Spatial pattern of global wetland carbon sequestration. **a**, Global map of mean annual wetland NEP between 2000 and 2020 at $0.25^\circ \times 0.25^\circ$ resolution, which was already weighted by grid cell areas. **b**, The latitudinal distribution of mean annual wetland NEP during 2000–2020. **c,d**, Box plots of the mean annual wetland net CO_2 uptake during 2000–2020 for the globe and across different climate zones (**c**), as well as different continents (**d**) ($n = 50$ RF models $\times 3$ wetland

area products). For each box plot, individual data points are shown as coloured dots. Centre lines inside the boxes represent means. Box boundaries represent the 75th and 25th quantiles, and whisker caps represent the 95th and 5th quantiles. **e**, Sankey diagram showing wetland C sink flows among three climate zones and six continents.

boosting (XGBoost) and support vector machine (SVM) (Supplementary Fig. 3). A new observation-based, global wetland net CO_2 uptake for 2000–2020 was estimated at 1,004 (95% CI 961 to 1,047) TgC yr^{-1} (Fig. 3c), accounting for ~30% of global land uptake and offsetting ~10% of anthropogenic emissions⁶. Regions exhibiting high wetland net CO_2 uptake included the Amazon River Basin, Pantanal, Congo River Basin, Okavango Delta, combined basins of Ganges, Brahmaputra and Meghna, and the Mississippi River Basin. These hotspots are characterized by high wetland WLs and extensive wetland areas (Extended Data Fig. 2a and Supplementary Fig. 1). By contrast, some peatlands located in tropical and boreal zones acted as net CO_2 sources (Fig. 3b), particularly in Southeast Asia and West Siberia Lowlands. Our dataset revealed that these peatlands commonly exhibited relatively low WLs (Extended Data Fig. 2a), which could facilitate aerobic decomposition of C-rich surface soils and subsequent CO_2 release^{28–30}. Tropical peatlands in Southeast Asia have also been threatened by frequent wildfires exacerbated by El Niño Southern Oscillation (ENSO) droughts and are therefore at great risk of becoming CO_2 sources^{30,55}. Similarly, C stored in West Siberia Lowland peatlands is increasingly threatened by permafrost thaw and climate warming, processes that accelerate decomposition and CO_2 emissions^{66–69}.

Across latitudes, higher values of wetland NEP were concentrated in the tropics (30°S – 30°N), with a net CO_2 uptake of 700 (95% CI 672 to 728) TgC yr^{-1} , accounting for 70% of global wetland C sequestration (Fig. 3c). In line with our findings, Mitsch et al.¹⁹ reported that tropical wetlands served as the largest net C sink, representing 67% of global wetland C sinks. Based on the compiled dataset, high WLs

are widespread in tropical wetlands (Extended Data Figs. 1b and 2a), reinforcing their dominant role in global wetland C retention. Furthermore, warmer climate, longer growing season and more diffuse light in the tropics hold the capacity to improve wetland C sinks^{7,51–53}. Apart from tropical wetlands, wetlands in northern mid-to-high latitudes ($>30^\circ \text{N}$) also sequestered large amounts of CO_2 from the atmosphere^{70,71}, accounting for 27% of global net CO_2 uptake. At the continental scale, South America, Asia and Africa emerged as the top three contributors to wetland C sequestration, collectively accounting for 79% of the global total (Fig. 3d). It should be noted that much of this uptake originated from tropical regions within these continents (Fig. 3e), where large wetland extents and consistently high WLs were prevalent (Extended Data Fig. 2a and Supplementary Fig. 1).

The analysis of the rate of change of NEP over time elucidated that 49% and 51% of global wetland grid cells showed increasing and decreasing trends, respectively (Fig. 4a). Sharp declines in wetland net CO_2 uptake rates were witnessed mainly in Amazon River Basin, Sumatra and Indochinese Peninsula, where WLs and precipitation typically displayed decreasing trends (Extended Data Fig. 2b and Supplementary Fig. 4). Over the past two decades, the Amazon has experienced frequent and severe droughts due to climate change (for example, warming anomaly of Tropical North Atlantic and ENSO). These droughts could favour wildfire occurrence and tree mortality, consequently undermining the region's C sink capacity^{72–75}. In Sumatra and Indochinese Peninsula wetlands, their C sink functions were strongly threatened by extensive peat oxidation and quasi-periodic ENSO droughts^{30,55,76,77}. By contrast, the marked enhancement of wetland C sequestration was

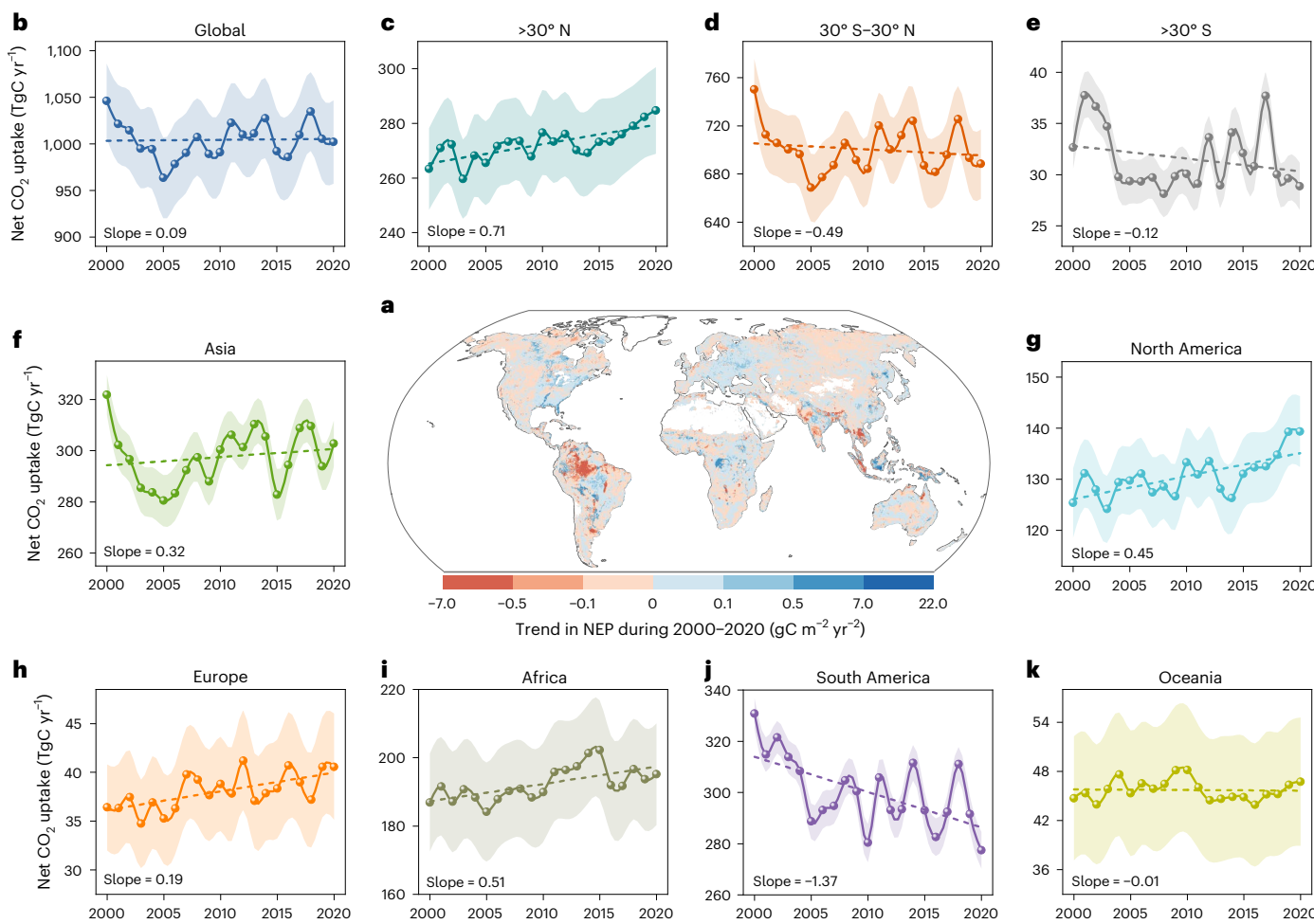


Fig. 4 | Temporal patterns in global and regional wetland carbon sequestration. **a**, A global explicit map of temporal trends in annual wetland NEP between 2000 and 2020 at $0.25^\circ \times 0.25^\circ$ resolution, which was already weighted by grid cell areas. **b–e**, Temporal changes in annual wetland net CO_2 uptake for the globe (**b**), $>30^\circ \text{N}$ (**c**), $30^\circ \text{S}-30^\circ \text{N}$ (**d**) and $>30^\circ \text{S}$ (**e**) over the period 2000–2020. The shadow areas represent the 95% CI based on 50 RF models and 3 wetland area products ($n = 50 \times 3$). Dashed coloured lines represent the

tendency lines fitted by linear regression models. **f–k**, Temporal variations in annual wetland net CO_2 uptake for Asia (**f**), North America (**g**), Europe (**h**), Africa (**i**), South America (**j**) and Oceania (**k**) during 2000–2020. The shadow areas represent the 95% CI based on 50 RF models and 3 wetland area products ($n = 50 \times 3$). Dashed coloured lines represent the tendency lines fitted by linear regression models.

primarily distributed in Eastern China, the Eastern USA, Eastern Europe, Hudson Bay Lowland, Congo River Basin, Borneo and Moxos Plains, where upward trends in WLs and precipitation were usually observed. In Eastern China, the Eastern USA, Eastern Europe and Hudson Bay Lowland, additional drivers included climate warming, extended growing seasons and enhanced ET^{7,21,78,79} (Supplementary Fig. 5), all of which favour higher NEP. In the Congo River Basin, wetland water storage increased since 2002 (ref. 80), providing more humid conditions that support C sequestration. Field monitoring has also confirmed that the C sink in Congo River Basin slightly increased in the three decades leading up to 2015, in contrast to the long-term decline observed in Amazon River Basin⁷⁵. In Borneo, rising wetland NEP was linked to the strong resilience of vegetation following environmental disturbance, with this resilience far exceeding that observed in both Amazon River and Congo River basins⁸¹.

Despite widespread regional changes in NEP, the annual net CO_2 uptake of global wetlands was relatively stable over the period 2000–2020, with a slight upward trend of 0.09 TgC yr^{-2} (Fig. 4b). Among climate zones, wetlands in northern mid-to-high latitudes exhibited a notable increasing CO_2 uptake rate of 0.71 TgC yr^{-2} (Fig. 4c), coinciding with rising precipitation and WL in this region (Extended Data Fig. 2b and Supplementary Fig. 4). Consistently, Peng et al.⁸²

demonstrated that wetland water storage increased in the Northern Hemisphere. In addition, regional climate warming, prolonged growing seasons and boosted ET have been observed in northern mid-to-high latitudes^{7,21,78,79} (Supplementary Fig. 5), all of which support the strengthening of wetland C sinks in this region. However, this increasing trend was almost entirely offset by decreasing wetland C sinks in the tropics and southern mid-to-high latitudes ($>30^\circ \text{S}$) (Fig. 4d,e). As discussed above, Amazon River Basin, Sumatra and Indochinese Peninsula were the hotspots for wetland NEP decline, collectively shaping the downward trend in tropical wetland net CO_2 uptake ($-0.49 \text{ TgC yr}^{-2}$). Across the continents, Africa showed the fastest increase in wetland C sequestration (0.51 TgC yr^{-2} ; Fig. 4i), followed by North America (0.45 TgC yr^{-2} ; Fig. 4g), Asia (0.32 TgC yr^{-2} ; Fig. 4f) and Europe (0.19 TgC yr^{-2} ; Fig. 4h). These increases were largely driven by increasing precipitation and WL in these four continents. Furthermore, wetlands in North America, Asia and Europe are predominantly located in northern mid-to-high latitudes, where climate warming, extended growing seasons and enhancement of ET are capable of boosting wetland C sink activity. By contrast, a sharp decline in wetland C sinks was observed in South America ($-1.37 \text{ TgC yr}^{-2}$; Fig. 4j), probably driven by decreases in precipitation and WL, which strongly weakened the region's relatively high baseline NEP.

More notably, global wetland net CO₂ uptake showed contrasting temporal variations between 2000–2005 and 2006–2020 (Fig. 4b). During 2000–2005, wetland C sink declines were widespread, especially in Amazon River Basin and Southeast Asia (Extended Data Fig. 7a). Due to the warming anomaly of Tropical North Atlantic, Amazon River Basin experienced a mega-drought in 2005 (ref. 74). Moreover, results from climate analysis for the period 1995–2005 revealed a steady decline in plant water availability over Amazon River Basin⁷². This drying climate caused a sharp drop in wetland net CO₂ uptake. In Southeast Asia, quasi-periodic ENSO droughts were the main contributor to attenuate wetland C sink activity between 2000 and 2005. During 2006–2020, Amazon River Basin, Sumatra and Indochinese Peninsula continued to see wetland C sink declines (Extended Data Fig. 7b), primarily due to post-drought vegetation mortality and reoccurrence of drought events^{72,74}. However, these losses were outweighed by increases in wetland C sinks in Eastern China, the Eastern USA, Eastern Europe, Hudson Bay Lowland, Congo River Basin, Borneo, Pampas and so on, resulting in an overall uptrend in global annual wetland net CO₂ uptake throughout 2006–2020.

Based on the estimates from Friedlingstein et al.⁶, the growth rates of terrestrial C sink decreased from 0.075 PgC yr⁻² ($P = 0.05$) during 1980–1999 to 0.037 PgC yr⁻² ($P = 0.18$) between 2000 and 2020 (Extended Data Fig. 8a). The temporal trajectory of global wetland net CO₂ uptake in this period exhibited a positive correlation with terrestrial C sinks and can explain 33% of temporal variations in terrestrial C sinks ($P = 0.008$; Extended Data Fig. 8b).

Limitations and uncertainties

Although this study compiled a comprehensive global wetland NEP dataset and provided valuable insights into spatiotemporal patterns of wetland C sequestration, several limitations and uncertainties must be acknowledged. First, while the dataset includes diverse climate zones and wetland types, most NEP measurements were concentrated in boreal and temperate regions. More field-based NEP data are urgently needed from Arctic and tropical zones, particularly for underrepresented wetland types such as peat swamps, swamps, seasonally or permanently inundated floodplains and wet tundras. Second, wetland CH₄ emissions have been previously estimated at 149 TgCH₄ yr⁻¹ (ref. 38), which directly weaken wetland Csinks by ~11% compared with net CO₂ uptake alone. Dissolved C losses through water export are also an important component of the wetland C budget, with large amounts of C transferred from freshwater wetlands to the ocean³⁹. Thus, wetland C sinks might be overestimated by our study owing to the exclusion of CH₄ emissions and dissolved C losses, which should be incorporated in future global wetland C budget assessments. Finally, our study focused on freshwater wetlands, and did not account for net CO₂ uptake from other aquatic ecosystems such as lakes, rivers, reservoirs, aquaculture ponds, mangroves, saltmarshes, tidal freshwater wetlands and so on. The C dynamics of these ecosystems warrant further investigation.

Methods

Wetland definition

Our definition of wetlands encompassed peatlands (bogs, fens and peat swamps), mineral soil wetlands (marshes and swamps), seasonal or permanent inundated floodplains and wet tundras (Supplementary Table 1). We excluded all open waters (for example, lakes, rivers, ponds and reservoirs), coastal wetlands (for example, mangroves, saltmarshes, seagrasses and tidal freshwater wetlands), drained wetlands (that is, wetlands drained for other land use types) and paddy fields. We defined wetland categories on the basis of a methodological rather than a priori definition or typology, that is, our operational wetland definition is inherited from the wetland maps we used⁸³. Global wetland area distributions were determined on the basis of the long-term maximum inundated area fraction (static wetland maps) from the following three sources: (1) WAD2M v.2.0 (13.6 Mkm²), produced from

multisensor remote sensing, and has successfully identified wetlands under dense canopies, excluding permanent water bodies, coastal wetlands, rice paddies and drained wetlands⁴⁰ (WAD2M v.2.0 covers the period 2000–2020 on a monthly scale at 0.25° × 0.25° spatial resolution); (2) GLWD v.2.0 (10.8 Mkm²), compiled from a selection of maps and charts, represents a static wetland map at 0.0041° × 0.0041° spatial resolution³¹ (GLWD v.2.0 classes 8 to 27 and 32 were selected and aggregated to 0.25° × 0.25° grid cells in our study, excluding open waters, coastal wetlands, paddy fields and drained wetlands); (3) GIEMS-MC (11.2 Mkm²), derived from the combination of GIEMS v.2.0 and GLWD v.2.0, included inundated and saturated wetlands and peatlands, excluding open water and paddy fields^{41,42}. To ensure comparability among the three wetland maps, we further subtracted coastal wetlands from GIEMS-MC by using GLWD v.2.0. GIEMS-MC was developed at 0.25° × 0.25° spatial resolution at a monthly time step for 1920–2020. These three products diverge in both the extent of global wetland area by 2.8 Mkm² (10.8–13.6 Mkm²; 24% of the average) and their geographic distribution (Supplementary Fig. 1) and have been adopted in the wetland C sink modelling framework to account for uncertainties in global wetland area estimates.

Compilation of the global wetland NEP database

The data used in our study were mainly collected by searching for literature studying wetland NEP through the Web of Science, Google Scholar and China National Knowledge Infrastructure in the period 1990–2024. The query terms for the literature search included ‘carbon dioxide OR CO₂ OR net ecosystem exchange OR NEE OR net ecosystem production OR NEP OR carbon OR primary production OR respiration OR greenhouse gas OR GHG OR global warming potential OR GWP’ AND ‘wetland OR inland wetland OR freshwater wetland OR peatland OR bog OR fen OR peat swamp OR mineral soil wetland OR marsh OR swamp OR floodplain OR tundra’. To avoid bias during publication selection, the following criteria were used to screen the literature: (1) only studies using the eddy covariance method and chamber-based method were selected; (2) studies using the chamber-based method were required to have at least three replicates; (3) field observations with experimental manipulation (for example, warming and fertilization) were excluded; (4) in situ monitoring need to have been carried out for at least one growing season (wetland sites that reported CO₂ fluxes for the growing season only were located in northern high-latitude zones; hence, we assigned non-growing season CO₂ fluxes using the estimates from Natali et al.⁸⁴); (5) multiyear observations within the same site were considered independent; (6) sites from open water, paddy fields, coastal wetlands and drained wetlands were excluded; (7) floodplains that have never been inundated were excluded. Detailed site-specific data such as latitude, longitude, measurement years, WLs, climate conditions, soil properties, plant variables and elevation were also extracted from the original publications. Data presented as figures and plots were identified using Web Plot Digitizer (version 3.11; <https://automeris.io/WebPlotDigitizer>). Wetland NEP and predictor variables collected from peer-reviewed publications were aggregated on an annual basis. In addition, we also extracted data from the FLUXNET database, which measures the fluxes of carbon, water and energy between the biosphere and atmosphere based on the eddy covariance method (<https://fluxnet.org/>). Database descriptions (for example, existing sites and gap filling) of the FLUXNET are described in detail by Pastorello et al.⁸⁵. We extracted wetland NEP and ancillary environmental variables (for example, WL) at each site and aggregated data at the annual scale. In total, our compiled database included 934 site–year records of wetland NEP observations collected from 258 peer-reviewed publications and the FLUXNET database, with observed years ranging from 1990 to 2023. These sites were distributed from 54.97° S to 81.80° N and from 157.41° W to 175.55° E, covering diverse climate zones and wetland types (Fig. 1). In addition, from our compiled dataset, we have screened out 663 paired observations that simultaneously measured NEP and

WLs (Supplementary Fig. 6), of which the WL data were subsequently included in the wetland WL modelling framework.

Compilation of the global wetland WL database

Data were obtained by searching for peer-reviewed articles studying wetland hydrological conditions that were published before 2024 using the Web of Science, Google Scholar and China National Knowledge Infrastructure; the keywords ‘water level OR water table OR water depth OR groundwater OR hydrology’ AND ‘wetland OR inland wetland OR freshwater wetland OR peatland OR bog OR fen OR peat swamp OR mineral soil wetland OR marsh OR swamp OR floodplain OR tundra’ were used in the searches. We utilized the following seven criteria to select publications: (1) the study was carried out in field conditions; (2) field observations with water-table manipulation experiments were excluded; (3) data simulated by the hydrological model were excluded; (4) the duration of the study was at least 1 year; (5) multiyear observations within the same site were considered independent; (6) sites from open water, paddy fields, coastal wetlands and drained wetlands were excluded; (7) floodplains that have never been inundated were excluded. Data on WLs, latitude, longitude, measurement years, climate conditions, soil properties, plant variables and elevation were extracted from the eligible literature. The software Web Plot Digitizer (version 3.11) was used to extract data from the graph. Finally, we compiled 2,295 site-year records of field observations of wetland WLs from 606 peer-reviewed publications, with observed years ranging from 1984 to 2023. Our compiled wetland WL dataset used in situ observations from 642 wetland sites across the globe that encompass various climate zones and wetland types (Extended Data Fig. 1). Of these, the vast majority of compiled WL data was measured manually or monitored through water-level sensors (for example, pressure transducer) with integrated data loggers and then corrected to the distance from the ground surface (positive data records denote WLs above the surface, and negative data records represent WLs below the surface). Sampling frequency largely depended on the type of wetland and associated environmental conditions, as well as sampling methods. Common sampling frequency included daily, weekly or semi-monthly intervals. Field measurements of WLs need to have been carried out for at least 1 year, to fully capture the seasonality of WL variations. Wetland WLs collected from peer-reviewed papers were aggregated on an annual basis. The annual mean WLs for the 2,295 observations ranged from approximately -100 to +100 cm, with the majority of observations between -50 and +30 cm (Supplementary Fig. 7), reflecting the water-level characteristics of global wetlands^{25,36}.

Global gridded environmental datasets

We used global gridded datasets representing climate, hydrology, topography, soil, plant and human disturbance to train the machine-learning models (Supplementary Table 2). Specifically, MAT and MAP were obtained from the CRU TS v4.05 (ref. 86). PAR and ET were acquired from the study by Tang et al.⁵² and Feng et al.⁸⁷, respectively. The elevation dataset was taken from WorldClim⁸⁸. Global gridded datasets of soil properties, including SOC, pH, BD, Clay, Sand, Silt, CEC and BS, were all collected from the SoilGRIDS database (<http://www.isric.org/explore/soilgrids>) and the Land-Atmosphere Interaction Research Group at Sun Yat-sen University (<http://global-change.bnu.edu.cn/research/soilw>). Canopy intercept and Runoff were obtained from the GLDAS-Noah v.2.1 dataset⁸⁹. In terms of plant variables, NDVI and EVI were derived from the MOD13C2 product (<https://earthdata.nasa.gov/>). Inundation fraction (fw) was extracted from the WAD2M v.2.0 dataset generated by Zhang et al.⁴⁰ and the GIEMS-MC dataset produced by Bernard et al.⁴¹. Wetland Loss was available from the study by Fluet-Chouinard et al.⁸³. Compound topographic index (CTI) and terrestrial groundwater table depth (WTD Fan) were obtained from the study by Marthews et al.⁹⁰ and Fan et al.³⁶, respectively. The spatial patterns of all global gridded environmental datasets

are shown in Supplementary Figs. 8–15. We resampled all the environmental layers into $0.25^\circ \times 0.25^\circ$ resolution before further analysis.

Development of machine-learning models

We randomly selected 80% of the samples from our compiled global-scale in situ database as the training set and the remaining 20% as the test set to diagnose the generalizability of machine-learning models as in ref. 91. We used a ‘grid search’ procedure on the entire training set to explore the parameter spaces of various machine-learning algorithms⁹², including RF, XGBoost and SVM. We performed the ‘hold-out’ method, in which the model was trained with 70% of the samples in the training set and validated on the remaining 30% (ref. 93). We used the training set to determine the best machine-learning algorithm and set of hyperparameters. We utilized the ‘mlr3verse’ package in R software to train machine-learning models. To evaluate the predictive performance of machine-learning models, we used the root mean square error (RMSE) and the coefficients of determination (R^2) values produced on the test set as the metrics.

Global extrapolation of WL and NEP

To determine the spatiotemporal variations in wetland WLs, we used the site-level wetland WL as the dependent variable and three climate variables (MAT, MAP and PAR), five hydrological variables (fw, ET, Canopy intercept, Runoff, and WTD Fan), four soil physical variables (BD, Clay, Sand and Silt), two plant variables (NDVI and EVI), two topographic variables (elevation and CTI), and Wetland Loss as candidate independent variables. Of these, fw, PAR, ET and MAT were the four most important drivers controlling wetland WL variations (Extended Data Fig. 5). To prevent the overfitting of machine-learning models, the final predictor variables were selected using the recursive feature elimination method. This approach can effectively reduce the number of predictor variables while maintaining the high predictive power of machine-learning models⁹⁴. Results of the recursive feature elimination method can be seen in Supplementary Fig. 16 and Supplementary Table 3. Initially, we assessed the performance of all three different machine-learning models (that is, RF, XGBoost and SVM) using the final predictor variables screened by the recursive feature elimination method. The results showed that the RF model performed best among all machine-learning models (Supplementary Fig. 7). In the model-testing phase, the R^2 and RMSE values for the RF model were 0.82 and 10.85, respectively. RF model is capable of accounting for nonlinear effects and complex interactions between predictors⁹⁵. Moreover, the RF model is well suited for handling small sample sizes and high-dimensional feature spaces without overfitting⁹². To map global wetland WLs at $0.25^\circ \times 0.25^\circ$ resolution during 2000–2020, we combined the training and test set to retrain the final RF model, using the same set of hyperparameters determined in the process of RF model development. Among the list of 17 candidate predictor variables, EVI, BD and Silt were excluded from training the final RF model (Supplementary Table 3). To obtain the uncertainty associated with predictions, we first repeated the RF model development 50 times to derive a series of hyperparameter sets. Next, we trained 50 RF models on all available samples using the 50 sets of hyperparameters. The average predicted map across 50 RF models was used as the final product, and the 95% CI was then considered as the indicator of prediction uncertainty. Uncertainties in the mapped mean annual wetland WLs are shown in Supplementary Fig. 17. To derive a global explicit map of temporal trend in annual wetland WLs between 2000 and 2020, we further used all spatial grid cells with 21 years of WLs and calculated slopes of wetland WLs over time using a separate linear regression model for each grid cell⁹⁶, and the 95% CI of the slope within each grid cell as the uncertainty of temporal trends. Uncertainties in the mapped temporal trends are shown in Supplementary Fig. 18. The global wetland WL dataset created by this study was subsequently used to simulate the wetland NEP variations.

To upscale field observations of wetland NEP to the global scale, the site-level wetland NEP was treated as the dependent variable and three climate variables (MAT, MAP and PAR), two hydrological variables (WL and ET), eight soil physicochemical variables (SOC, pH, BD, Clay, Sand, Silt, CEC and BS), two plant variables (NDVI and EVI) and elevation were considered as the candidate independent variables. We used the recursive feature elimination method to reduce the number of predictor variables, but still ensured a high predictive power of machine-learning models. Results of the recursive feature elimination method are shown in Supplementary Fig. 19 and Supplementary Table 4. Utilizing the final predictor variables selected by the recursive feature elimination method, we evaluated the performance of three machine-learning models, that is, RF, XGBoost and SVM. Among them, the RF model outperformed the other two methods, with an R^2 and RMSE of 0.84 and 86.36, respectively (Supplementary Fig. 3). We combined the training and test set to retrain the final RF model using the same set of hyperparameters derived from the RF model development, to map global wetland NEP with a $0.25^\circ \times 0.25^\circ$ resolution during 2000–2020. Among the list of 16 candidate predictor variables, EVI and BD were excluded from training the final RF model (Supplementary Table 4). Furthermore, we repeated the RF model development 50 times to determine a series of hyperparameter sets, which were subsequently used to train 50 RF models on all available samples. Notably, annual wetland C sequestration was estimated by multiplying annual wetland NEP by the annual wetland area at $0.25^\circ \times 0.25^\circ$ resolution. Accordingly, our wetland C sink modelling framework also accounted for uncertainties in global wetland area estimates. In total, we had 150 (50 RF models \times 3 wetland area products) ensemble members and treated the average predicted map as the final product. The 95% CI was then considered as the indicator of prediction uncertainty. Uncertainties in the mapped mean annual wetland C sequestration are shown in Supplementary Fig. 20. Moreover, based on all spatial grid cells with 21 years of wetland NEP, we calculated slopes of NEP over time using a separate linear regression model for each grid cell to construct a global explicit map of temporal trend in annual wetland NEP during 2000–2020, and the 95% CI of the slope within each grid cell was used as the uncertainty of temporal trends. Uncertainties in the mapped temporal trends are shown in Supplementary Fig. 21.

Statistical analyses

All statistical analyses were performed using R v.4.1.0 (ref. 97). Data were examined for normality and homogeneity and log-transformed as necessary to satisfy the assumptions of normality. One-way analysis of variance and least significant difference multiple comparisons were used to test the differences in WL and NEP among climate zones and wetland types through the package ‘agricolae’. By using the R package ‘caret’, we conducted the recursive feature elimination to prevent the overfitting of machine-learning models. The relative importance of each predictor variable was determined by the RF model using the ‘impurity’ method⁹⁸. The nonlinear relationship between NEP and WL was detected using the ‘partialplot’ function in the R package ‘randomForest’. Linear mixed-effect models were performed with the ‘lme4’ package of R.

Reporting summary

Further information on research design is available in the Nature Portfolio Reporting Summary linked to this article.

Data availability

The WAD2M v.2.0 dataset is available via Zenodo at <https://doi.org/10.5281/zenodo.3998453> (ref. 99). The GIEMS-MC dataset is available via Zenodo at <https://doi.org/10.5281/zenodo.13919644> (ref. 100). The GLWD v.2.0 dataset is available via Figshare at <https://figshare.com/s/e40017f69f41f80d50df> (ref. 101). The FLUXNET database is available at <https://fluxnet.org/data/fluxnet2015-dataset/>. MAT and MAP were obtained from https://crudata.uea.ac.uk/cru/data/hrg/cru_ts_4.05/.

PAR originated from <https://doi.org/10.11888/RemoteSen.tpd.271909>. ET was extracted from <https://doi.org/10.57760/sciedb.10519>. Elevation was taken from <https://worldclim.org/data/worldclim21.html>. Global gridded datasets of soil properties, including SOC, pH, BD, Clay, Sand, Silt, CEC and BS, were all collected from the SoilGRIDS database (<http://www.isric.org/explore/soilgrids>) and the Land-Atmosphere Interaction Research Group at Sun Yat-sen University (<http://globalchange.bnu.edu.cn/research/soilw>). Canopy intercept and Runoff were obtained from https://search.earthdata.nasa.gov/search?q=GLDAS_NOAH025_M_2.1. NDVI and EVI were derived from <https://earthdata.nasa.gov/>. Wetland Loss data are available via Zenodo at <https://doi.org/10.5281/zenodo.7293597> (ref. 102). CTI can be downloaded at <https://doi.org/10.5066/F7S180ZP>. WTD Fan was obtained from <http://thredds-gfnl.usc.es/thredds/catalog/GLOBALWTDFTP/annualmeans/catalog.html>. Our compiled datasets of wetland NEP and WL are available via Figshare at <https://doi.org/10.6084/m9.figshare.26825293> (ref. 103). Source data are provided with this paper.

Code availability

Code used to reproduce the findings of this work can be obtained at <https://doi.org/10.24433/CO.7249484.v1>.

References

- IPCC Climate Change 2021: The Physical Science Basis. Contribution of Working Group I to the Sixth Assessment Report of the Intergovernmental Panel on Climate Change (eds Masson-Delmotte, V. et al.) (Cambridge Univ. Press, 2021).
- Prentice, I. C. et al. The carbon cycle and atmospheric carbon dioxide. in *Climate Change 2001: The Scientific Basis. Contribution of Working Group I to the Third Assessment Report of the Intergovernmental Panel on Climate Change* (eds Houghton, J. T. et al.) 183–237 (Cambridge Univ. Press, 2001).
- Lan, X., Tans, P. & Thoning, K. W. Trends in Atmospheric Carbon Dioxide (National Oceanic and Atmospheric Administration, Global Monitoring Laboratory, 2024); <https://doi.org/10.15138/9NOH-ZH07>
- Canadell, J. G. et al. Contributions to accelerating atmospheric CO₂ growth from economic activity, carbon intensity, and efficiency of natural sinks. *Proc. Natl Acad. Sci. USA* **104**, 18866–18870 (2007).
- Falkowski, P. et al. The global carbon cycle: a test of our knowledge of earth as a system. *Science* **290**, 291–296 (2000).
- Friedlingstein, P. et al. Global Carbon Budget 2023. *Earth. Syst. Sci. Data* **15**, 5301–5369 (2023).
- Ruehr, S. et al. Evidence and attribution of the enhanced land carbon sink. *Nat. Rev. Earth Environ.* **4**, 518–534 (2023).
- Chen, C., Riley, W. J., Prentice, I. C. & Keenan, T. F. CO₂ fertilization of terrestrial photosynthesis inferred from site to global scales. *Proc. Natl Acad. Sci. USA* **119**, e2115627119 (2022).
- Galloway, J. N., Bleeker, A. & Erisman, J. W. The human creation and use of reactive nitrogen: a global and regional perspective. *Annu. Rev. Environ. Resour.* **46**, 255–288 (2021).
- Piao, S. et al. Spatiotemporal patterns of terrestrial carbon cycle during the 20th century. *Glob. Biogeochem. Cycle* **23**, GB4026 (2009).
- Piao, S. et al. Plant phenology and global climate change: current progresses and challenges. *Glob. Change Biol.* **25**, 1922–1940 (2019).
- Penuelas, J. Decreasing efficiency and slowdown of the increase in terrestrial carbon-sink activity. *One Earth* **6**, 591–594 (2023).
- Wang, S. et al. Recent global decline of CO₂ fertilization effects on vegetation photosynthesis. *Science* **370**, 1295–1300 (2020).

14. Davidson, N. C., Fluet-Chouinard, E. & Finlayson, C. M. Global extent and distribution of wetlands: trends and issues. *Mar. Freshw. Res.* **69**, 620–627 (2018).
15. Lal, R. Carbon sequestration. *Philos. Trans. R. Soc. B* **363**, 815–830 (2008).
16. Poulter, B. et al. in *Wetland Carbon and Environmental Management* (eds Krauss, K. W., Zhu, Z. & Stagg, C. L.) 1–20 (Wiley, 2021).
17. Xiao, D., Deng, L., Kim, D. G., Huang, C. & Tian, K. Carbon budgets of wetland ecosystems in China. *Glob. Change Biol.* **25**, 2061–2076 (2019).
18. Li, J. et al. Convergence of carbon sink magnitude and water table depth in global wetlands. *Ecol. Lett.* **26**, 797–804 (2023).
19. Mitsch, W. J. et al. Wetlands, carbon, and climate change. *Landscape Ecol.* **28**, 583–597 (2012).
20. Mitsch, W. J. & Gosselink, J. G. *Wetlands* 5th edn (Wiley, 2015).
21. Bao, T., Jia, G. & Xu, X. Weakening greenhouse gas sink of pristine wetlands under warming. *Nat. Clim. Chang.* **13**, 462–469 (2023).
22. Wang, L. et al. Net exchanges of CO₂, CH₄ and N₂O between marshland and the atmosphere in Northeast China as influenced by multiple global environmental changes. *Atmos. Environ.* **63**, 77–85 (2012).
23. Wang, H. et al. Molecular mechanisms of water table lowering and nitrogen deposition in affecting greenhouse gas emissions from a Tibetan alpine wetland. *Glob. Change Biol.* **23**, 815–829 (2017).
24. Mitsch, W. J. et al. Tropical wetlands: seasonal hydrologic pulsing, carbon sequestration, and methane emissions. *Wetl. Ecol. Manag.* **18**, 573–586 (2010).
25. Zou, J. et al. Rewetting global wetlands effectively reduces major greenhouse gas emissions. *Nat. Geosci.* **15**, 627–632 (2022).
26. Evans, C. D. et al. Overriding water table control on managed peatland greenhouse gas emissions. *Nature* **593**, 548–552 (2021).
27. Huang, Y. et al. Tradeoff of CO₂ and CH₄ emissions from global peatlands under water-table drawdown. *Nat. Clim. Chang.* **11**, 618–622 (2021).
28. Ise, T., Dunn, A. L., Wofsy, S. C. & Moorcroft, P. R. High sensitivity of peat decomposition to climate change through water-table feedback. *Nat. Geosci.* **1**, 763–766 (2008).
29. Kwon, M. J. et al. Lowering water table reduces carbon sink strength and carbon stocks in northern peatlands. *Glob. Change Biol.* **28**, 6752–6770 (2022).
30. Deshmukh, C. S. et al. Conservation slows down emission increase from a tropical peatland in Indonesia. *Nat. Geosci.* **14**, 484–490 (2021).
31. Lehner, B. et al. Mapping the world's inland surface waters: an update to the Global Lakes and Wetlands Database (GLWD v2). *Earth. Syst. Sci. Data Discuss.* **2024**, 1–49 (2024).
32. Laiho, R. Decomposition in peatlands: reconciling seemingly contrasting results on the impacts of lowered water levels. *Soil Biol. Biochem.* **38**, 2011–2024 (2006).
33. Sulman, B. N. et al. CO₂ fluxes at northern fens and bogs have opposite responses to inter-annual fluctuations in water table. *Geophys. Res. Lett.* **37**, L19702 (2010).
34. Grant, R. F., Desai, A. R. & Sulman, B. N. Modelling contrasting responses of wetland productivity to changes in water table depth. *Biogeosciences* **9**, 4215–4231 (2012).
35. Ouyang, X., Maher, D. T. & Santos, I. R. Climate change decreases groundwater carbon discharges in global tidal wetlands. *One Earth* **7**, 1442–1455 (2024).
36. Fan, Y., Li, H. & Miguez-Macho, G. Global patterns of groundwater table depth. *Science* **339**, 940–943 (2013).
37. Schrier-Uijl, A. P. et al. Comparison of chamber and eddy covariance-based CO₂ and CH₄ emission estimates in a heterogeneous grass ecosystem on peat. *Agric. For. Meteorol.* **150**, 825–831 (2010).
38. Saunois, M. et al. The global methane budget 2000–2017. *Earth. Syst. Sci. Data* **12**, 1561–1623 (2020).
39. Pilla, R. M. et al. Anthropogenically driven climate and landscape change effects on inland water carbon dynamics: what have we learned and where are we going? *Glob. Change Biol.* **28**, 5601–5629 (2022).
40. Zhang, Z. et al. Development of the global dataset of Wetland Area and Dynamics for Methane Modeling (WAD2M). *Earth. Syst. Sci. Data* **13**, 2001–2023 (2021).
41. Bernard, J. et al. The GIEMS-MethaneCentric database: a dynamic and comprehensive global product of methane-emitting aquatic areas. *Earth. Syst. Sci. Data Discuss.* **2024**, 1–35 (2024).
42. Prigent, C., Jimenez, C. & Bousquet, P. Satellite-derived global surface water extent and dynamics over the last 25 years (GIEMS-2). *J. Geophys. Res. Atmos.* **125**, e2019JD030711 (2020).
43. Lu, W. et al. Contrasting ecosystem CO₂ fluxes of inland and coastal wetlands: a meta-analysis of eddy covariance data. *Glob. Change Biol.* **23**, 1180–1198 (2017).
44. Maas, C. J. M. & Hox, J. J. Sufficient sample sizes for multilevel modeling. *Methodology* **1**, 86–92 (2005).
45. Rocha, A. V. & Goulden, M. L. Why is marsh productivity so high? New insights from eddy covariance and biomass measurements in a *Typha* marsh. *Agric. For. Meteorol.* **149**, 159–168 (2009).
46. Li, J. et al. Radiative forcing of methane emission completely offsets net carbon dioxide uptake in a temperate freshwater marsh from the present to future. *Agric. For. Meteorol.* **346**, 109889 (2024).
47. Raymond, P. A. et al. Global carbon dioxide emissions from inland waters. *Nature* **503**, 355–359 (2013).
48. Lauerwald, R., Laruelle, G. G., Hartmann, J., Ciais, P. & Regnier, P. A. Spatial patterns in CO₂ evasion from the global river network. *Glob. Biogeochem. Cycle* **29**, 534–554 (2015).
49. Hwang, Y. et al. Comprehensive assessments of carbon dynamics in an intermittently-irrigated rice paddy. *Agric. For. Meteorol.* **285**, 107933 (2020).
50. Knox, S. H. et al. Agricultural peatland restoration: effects of land-use change on greenhouse gas (CO₂ and CH₄) fluxes in the Sacramento-San Joaquin Delta. *Glob. Change Biol.* **21**, 750–765 (2015).
51. Garonna, I., de Jong, R. & Schaepman, M. E. Variability and evolution of global land surface phenology over the past three decades (1982–2012). *Glob. Change Biol.* **22**, 1456–1468 (2016).
52. Tang, W., Qin, J., Yang, K., Jiang, Y. & Pan, W. Mapping long-term and high-resolution global gridded photosynthetically active radiation using the ISCCP H-series cloud product and reanalysis data. *Earth. Syst. Sci. Data* **14**, 2007–2019 (2022).
53. Gallego-Sala, A. V. et al. Latitudinal limits to the predicted increase of the peatland carbon sink with warming. *Nat. Clim. Chang.* **8**, 907–913 (2018).
54. Dalmagro, H. J. et al. Radiative forcing of methane fluxes offsets net carbon dioxide uptake for a tropical flooded forest. *Glob. Change Biol.* **25**, 1967–1981 (2019).
55. Hirano, T. et al. Large variation in carbon dioxide emissions from tropical peat swamp forests due to disturbances. *Commun. Earth Environ.* **5**, 221 (2024).
56. Yu, Z. et al. Peatlands and their role in the global carbon cycle. *Eos* **92**, 97–98 (2011).
57. Ribeiro, K. et al. Tropical peatlands and their contribution to the global carbon cycle and climate change. *Glob. Change Biol.* **27**, 489–505 (2021).
58. Greenwell, B. M. pdp: an R package for constructing partial dependence plots. *R. J.* **9**, 421–436 (2017).
59. Chen, H., Xu, X., Fang, C., Li, B. & Nie, M. Differences in the temperature dependence of wetland CO₂ and CH₄ emissions vary with water table depth. *Nat. Clim. Chang.* **11**, 766–771 (2021).
60. Wei, S. et al. Climate warming negatively affects plant water-use efficiency in a seasonal hydroperiod wetland. *Water Res.* **242**, 120246 (2023).

61. Naeem, S. et al. Recent change in ecosystem water use efficiency in China mainly dominated by vegetation greening and increased CO₂. *Remote Sens. Environ.* **298**, 113811 (2023).
62. Crous, K. Y. Plant responses to climate warming: physiological adjustments and implications for plant functioning in a future, warmer world. *Am. J. Bot.* **106**, 1049–1051 (2019).
63. Koven, C. D. et al. Permafrost carbon-climate feedbacks accelerate global warming. *Proc. Natl Acad. Sci. USA* **108**, 14769–14774 (2011).
64. Liu, Z. et al. Respiratory loss during late-growing season determines the net carbon dioxide sink in northern permafrost regions. *Nat. Commun.* **13**, 5626 (2022).
65. Wang, Y. et al. Beyond the visible: accounting for ultraviolet and far-red radiation in vegetation productivity and surface energy budgets. *Glob. Change Biol.* **30**, e17346 (2024).
66. Hugelius, G. et al. Large stocks of peatland carbon and nitrogen are vulnerable to permafrost thaw. *Proc. Natl Acad. Sci. USA* **117**, 20438–20446 (2020).
67. Fewster, R. E. et al. Imminent loss of climate space for permafrost peatlands in Europe and Western Siberia. *Nat. Clim. Chang.* **12**, 373–379 (2022).
68. Vasiliev, A. A. et al. Permafrost degradation in the western Russian arctic. *Environ. Res. Lett.* **15**, 045001 (2020).
69. Serikova, S. et al. High carbon emissions from thermokarst lakes of Western Siberia. *Nat. Commun.* **10**, 1552 (2019).
70. Virkkala, A. M. et al. Statistical upscaling of ecosystem CO₂ fluxes across the terrestrial tundra and boreal domain: regional patterns and uncertainties. *Glob. Change Biol.* **27**, 4040–4059 (2021).
71. Nahlik, A. M. & Fennessy, M. S. Carbon storage in US wetlands. *Nat. Commun.* **7**, 13835 (2016).
72. Saatchi, S. et al. Persistent effects of a severe drought on Amazonian forest canopy. *Proc. Natl Acad. Sci. USA* **110**, 565–570 (2013).
73. Brienen, R. J. et al. Long-term decline of the Amazon carbon sink. *Nature* **519**, 344–348 (2015).
74. Yang, Y. et al. Post-drought decline of the Amazon carbon sink. *Nat. Commun.* **9**, 3172 (2018).
75. Hubau, W. et al. Asynchronous carbon sink saturation in African and Amazonian tropical forests. *Nature* **579**, 80–87 (2020).
76. Dommain, R., Couwenberg, J., Glaser, P. H., Joosten, H. & Suryadiputra, I. N. N. Carbon storage and release in Indonesian peatlands since the last deglaciation. *Quat. Sci. Rev.* **97**, 1–32 (2014).
77. Miettinen, J., Hooijer, A., Vernimmen, R., Liew, S. C. & Page, S. E. From carbon sink to carbon source: extensive peat oxidation in insular Southeast Asia since 1990. *Environ. Res. Lett.* **12**, 024014 (2017).
78. Jeong, S. J., HO, C. H., GIM, H. J. & Brown, M. E. Phenology shifts at start vs. end of growing season in temperate vegetation over the Northern Hemisphere for the period 1982–2008. *Glob. Change Biol.* **17**, 2385–2399 (2011).
79. Buermann, W. et al. Widespread seasonal compensation effects of spring warming on northern plant productivity. *Nature* **562**, 110–114 (2018).
80. Tourian, M. J. et al. Current availability and distribution of Congo Basin's freshwater resources. *Commun. Earth Environ.* **4**, 174 (2023).
81. Heinrich, V. H. et al. The carbon sink of secondary and degraded humid tropical forests. *Nature* **615**, 436–442 (2023).
82. Peng, S. et al. Wetland emission and atmospheric sink changes explain methane growth in 2020. *Nature* **612**, 477–482 (2022).
83. Fluet-Chouinard, E. et al. Extensive global wetland loss over the past three centuries. *Nature* **614**, 281–286 (2023).
84. Natali, S. M. et al. Large loss of CO₂ in winter observed across the northern permafrost region. *Nat. Clim. Chang.* **9**, 852–857 (2019).
85. Pastorello, G. et al. The FLUXNET2015 dataset and the ONEFlux processing pipeline for eddy covariance data. *Sci. Data* **7**, 225 (2020).
86. Harris, I., Osborn, T. J., Jones, P. & Lister, D. Version 4 of the CRU TS monthly high-resolution gridded multivariate climate dataset. *Sci. Data* **7**, 109 (2020).
87. Feng, Q. et al. Long-term gridded land evapotranspiration reconstruction using Deep Forest with high generalizability. *Sci. Data* **10**, 908 (2023).
88. Fick, S. E. & Hijmans, R. J. WorldClim 2: new 1-km spatial resolution climate surfaces for global land areas. *Int. J. Climatol.* **37**, 4302–4315 (2017).
89. Rodell, M. et al. The global land data assimilation system. *Bull. Am. Meteorol. Soc.* **85**, 381–394 (2004).
90. Marthews, T. R., Dadson, S. J., Lehner, B., Abele, S. & Gedney, N. High-resolution global topographic index values for use in large-scale hydrological modeling. *Hydrol. Earth Syst. Sci.* **19**, 91–104 (2015).
91. Hu, H. et al. Relative increases in CH₄ and CO₂ emissions from wetlands under global warming dependent on soil carbon substrates. *Nat. Geosci.* **17**, 26–31 (2024).
92. Xu, P. et al. Fertilizer management for global ammonia emission reduction. *Nature* **626**, 792–798 (2024).
93. Bischl, B., Mersmann, O., Trautmann, H. & Weihs, C. Resampling methods for meta-model validation with recommendations for evolutionary computation. *Evol. Comput.* **20**, 249–275 (2012).
94. Darst, B. F., Malecki, K. C. & Engelman, C. D. Using recursive feature elimination in random forest to account for correlated variables in high dimensional data. *BMC Genet.* **19**, 1–6 (2018).
95. Breiman, L. Random forests. *Mach. Learn.* **45**, 5–32 (2001).
96. Patoine, G. et al. Drivers and trends of global soil microbial carbon over two decades. *Nat. Commun.* **13**, 4195 (2022).
97. R Core Team. *R: A Language and Environment for Statistical Computing* (R Foundation for Statistical Computing, 2021).
98. Ren, S., Wang, C. & Zhou, Z. Global distributions of reactive iron and aluminum influence the spatial variation of soil organic carbon. *Glob. Change Biol.* **30**, e17576 (2024).
99. Zhang, Z. et al. Development of a global dataset of Wetland Area and Dynamics for Methane Modeling (WAD2M). Zenodo <https://doi.org/10.5281/zenodo.3998453> (2021).
100. Bernard, J. et al. GIEMS-MethaneCentric. Zenodo <https://doi.org/10.5281/zenodo.13919644> (2024).
101. Lehner, B. et al. Global Lakes and Wetlands Database (GLWD) version 2.0. Figshare <https://doi.org/10.6084/m9.figshare.28519994.v1> (2025).
102. Fluet-Chouinard, E. et al. Global wetland loss reconstruction over 1700–2020. Zenodo <https://doi.org/10.5281/zenodo.7293597> (2022).
103. Li, J. et al. Two decades of improved wetland carbon sequestration in northern mid-high latitudes offset by tropical and southern declines. Figshare <https://doi.org/10.6084/m9.figshare.26825293> (2025).
104. Liu, L. et al. Increasingly negative tropical water-interannual CO₂ growth rate coupling. *Nature* **618**, 755–760 (2023).

Acknowledgements

This work was financially supported by the National Natural Science Foundation of China (grant nos. 42322709, 42177301 and U24A20628), the Natural Science Foundation (BK20230050), Carbon Peak & Carbon Neutral Science and Technology Innovation Project of Jiangsu Province (BK20220020) and the Chinese Academy of Sciences Project for Young Scientists in Basic Research (YSBR-089).

Author contributions

J.Y., W.D. and J.L. designed the research. J.L., P.C., H.K., C.F., Y.H., Y.D., D.L. and Y.L. performed the data extraction and analysis. J.L. wrote the first draft of the paper, with all authors contributing to the revisions.

Competing interests

The authors declare no competing interests.

Additional information

Extended data is available for this paper at
<https://doi.org/10.1038/s41559-025-02809-1>.

Supplementary information The online version contains supplementary material available at
<https://doi.org/10.1038/s41559-025-02809-1>.

Correspondence and requests for materials should be addressed to Junji Yuan or Weixin Ding.

Peer review information *Nature Ecology & Evolution* thanks Xiaoguang Ouyang and Carl Trettin for their contribution to the peer review of this work.

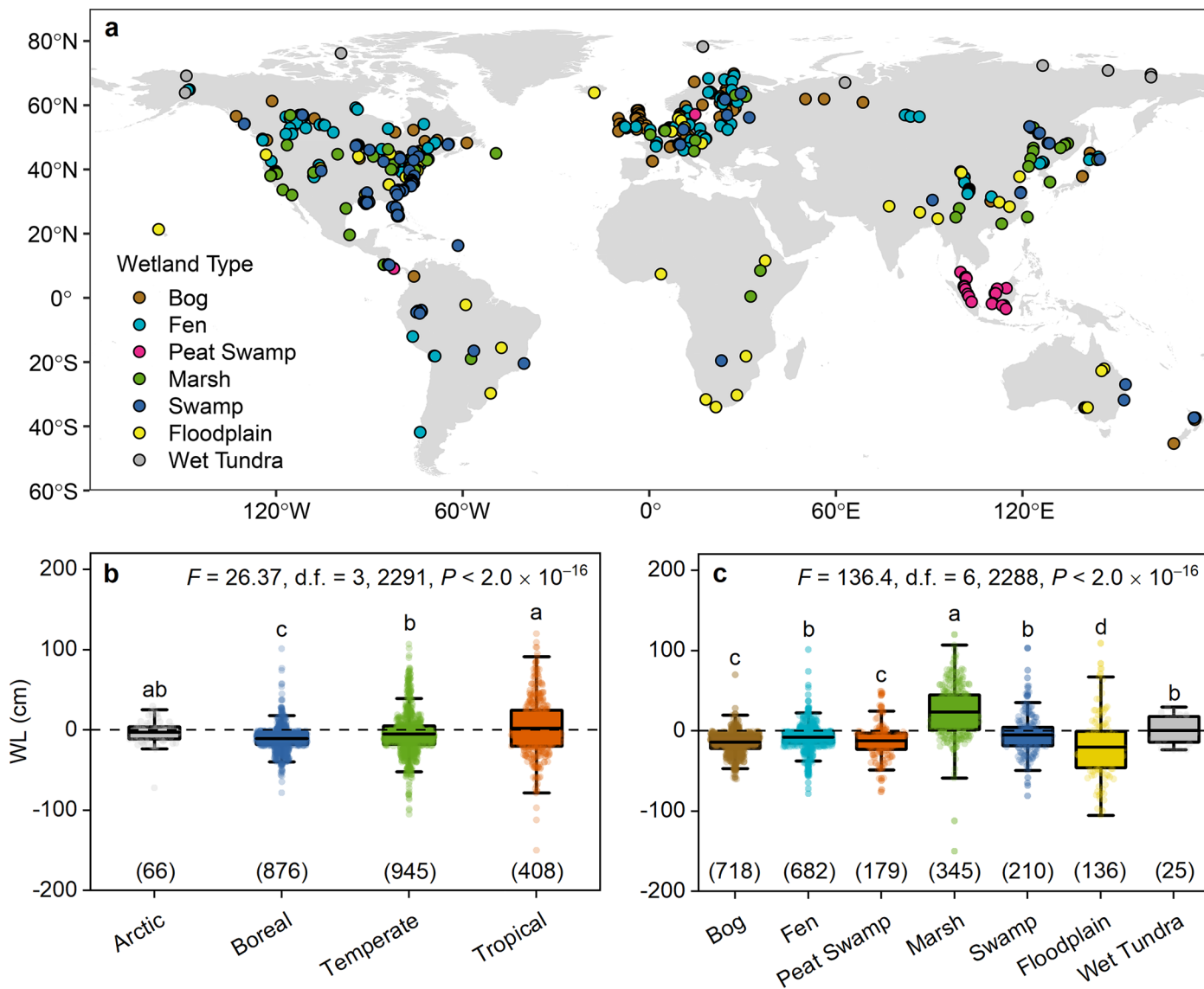
Reprints and permissions information is available at www.nature.com/reprints.

Publisher's note Springer Nature remains neutral with regard to jurisdictional claims in published maps and institutional affiliations.

Springer Nature or its licensor (e.g. a society or other partner) holds exclusive rights to this article under a publishing agreement with the author(s) or other rightsholder(s); author self-archiving of the accepted manuscript version of this article is solely governed by the terms of such publishing agreement and applicable law.

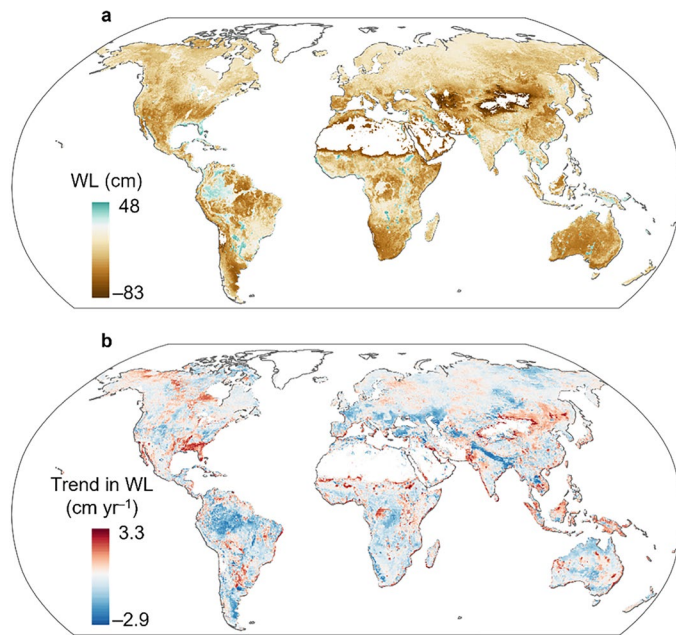
© The Author(s), under exclusive licence to Springer Nature Limited 2025

¹State Key Laboratory of Soil and Sustainable Agriculture, Institute of Soil Science, Chinese Academy of Sciences, Nanjing, China. ²University of Chinese Academy of Sciences, Beijing, China. ³Laboratoire des Sciences du Climat et de l'Environnement, LSCE/IPSL, CEA-CNRS-UVSQ, Université Paris-Saclay, Gif-sur-Yvette, France. ⁴Yellow River Research Institute, North China University of Water Resources and Electric Power, Zhengzhou, China. ⁵School of Natural Sciences, Bangor University, Gwynedd, UK. ⁶Key Laboratory of Ecosystem Network Observation and Modeling, Institute of Geographic Sciences and Natural Resources Research, Chinese Academy of Sciences, Beijing, China. ⁷Co-Innovation Center for Sustainable Forestry in Southern China, Nanjing Forestry University, Nanjing, China.  e-mail: jjyuan@issas.ac.cn; wxding@issas.ac.cn

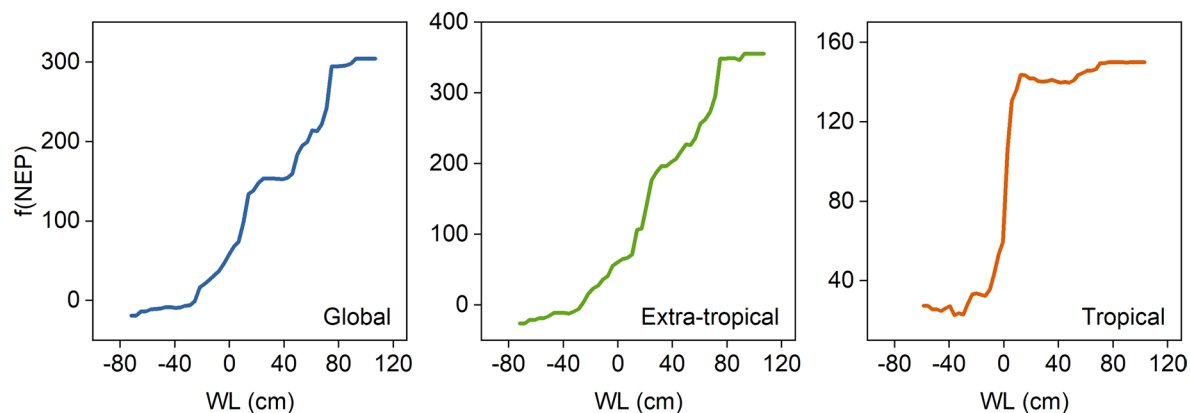


Extended Data Fig. 1 | Characteristics of global wetland water level (WL).
a Global distribution of field observations of wetland WL included in our compiled dataset. The wetland types are shown as colored dots. **b, c** Box plots of wetland WL in different climate zones (**b**) and wetland types (**c**). Note here that the definition of floodplain represents seasonal or permanent inundated floodplain. For each box plot, individual data points are shown as colored dots. Center lines

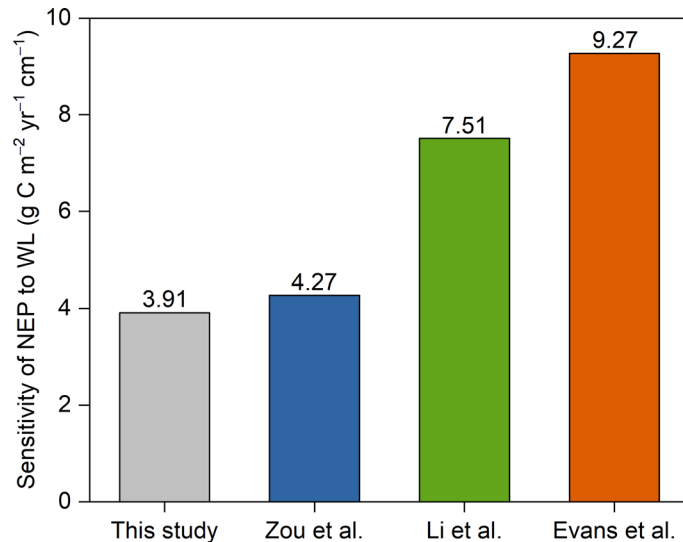
inside the boxes represent means. Box boundaries represent the 75th and 25th quantiles, whisker caps represent the 95th and 5th quantiles. Different lowercase letters indicate significant differences at $\alpha = 0.05$, as determined by using one-way ANOVA and LSD tests. No adjustments were made for multiple comparisons. Numbers in parentheses next to the x-axis indicate sample sizes (n).



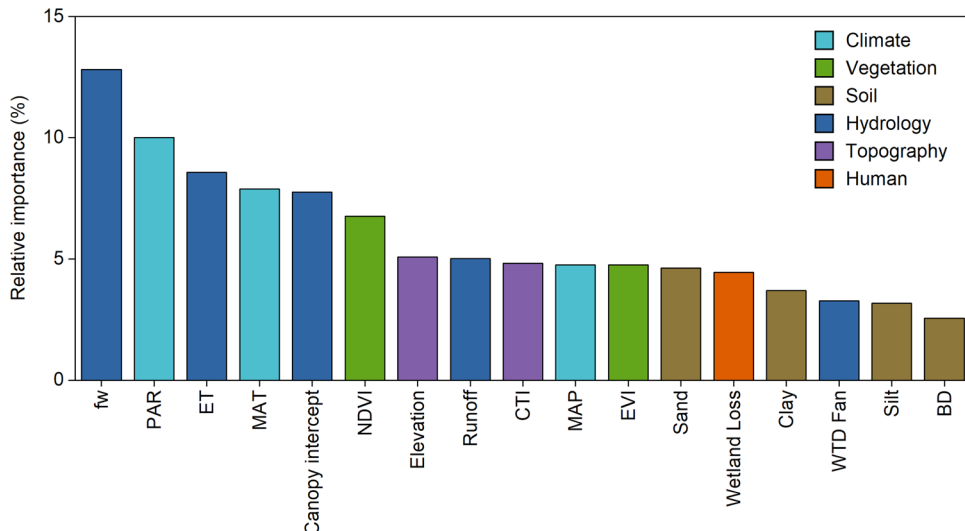
Extended Data Fig. 2 | Spatiotemporal pattern of global wetland water level (WL). **a** Global map of mean annual wetland WL between 2000 and 2020 at $0.25^\circ \times 0.25^\circ$ resolution. **b** Global distribution of temporal trends in annual wetland WL during 2000–2020 at $0.25^\circ \times 0.25^\circ$ resolution.



Extended Data Fig. 3 | Non-linear responses of net ecosystem production (NEP) to water level (WL) for global wetlands and wetlands in extra-tropical and tropical regions. The y-axis denotes the marginal effect of WL on the predicted NEP (that is, $f(\text{NEP})$), while holding all other predictors constant. $f(\text{NEP})$ was detected by the partial dependence plot from the random forest model.

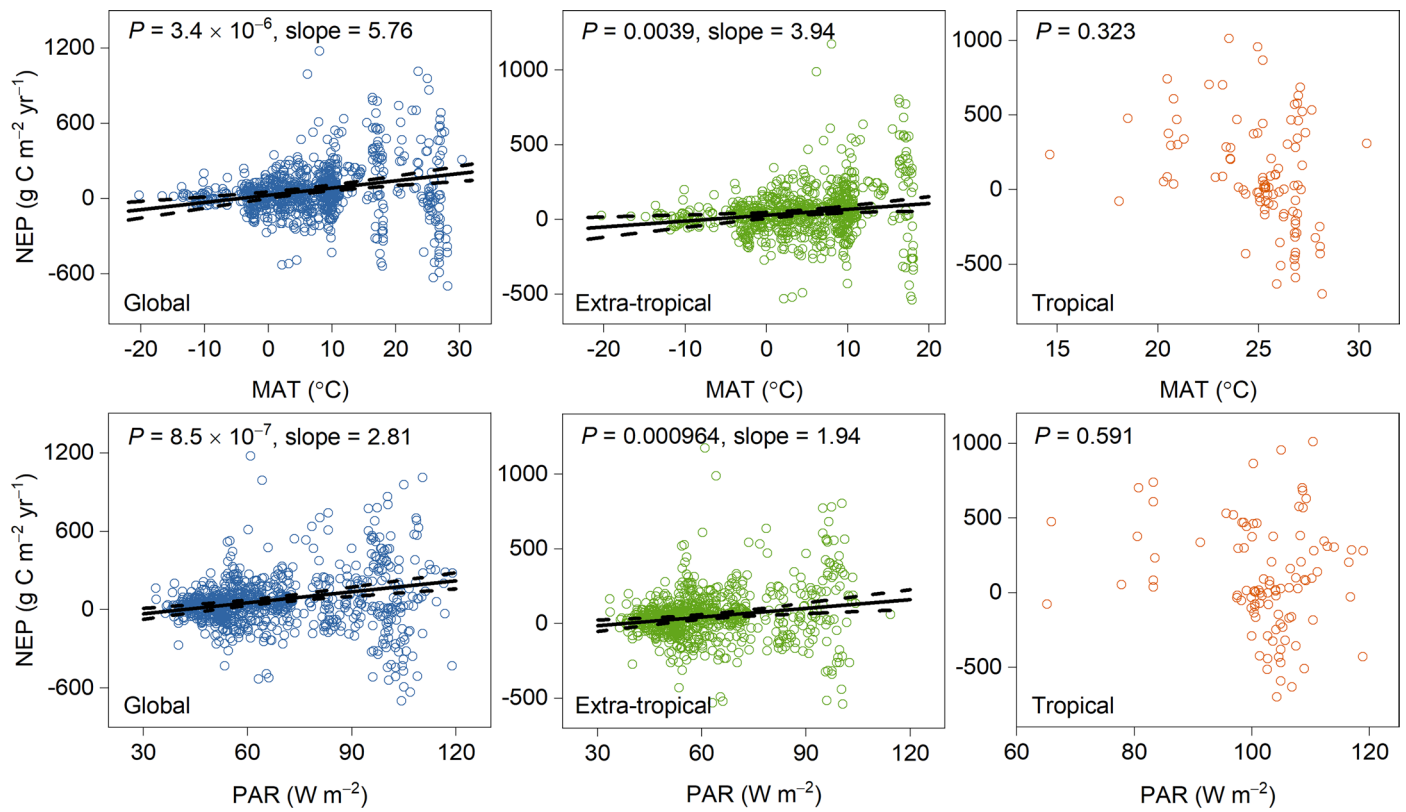


Extended Data Fig. 4 | Comparison of the sensitivity of net ecosystem production (NEP) to water level (WL) obtained in this study with Zou et al.²⁵, Li et al.¹⁸, and Evans et al.²⁶.



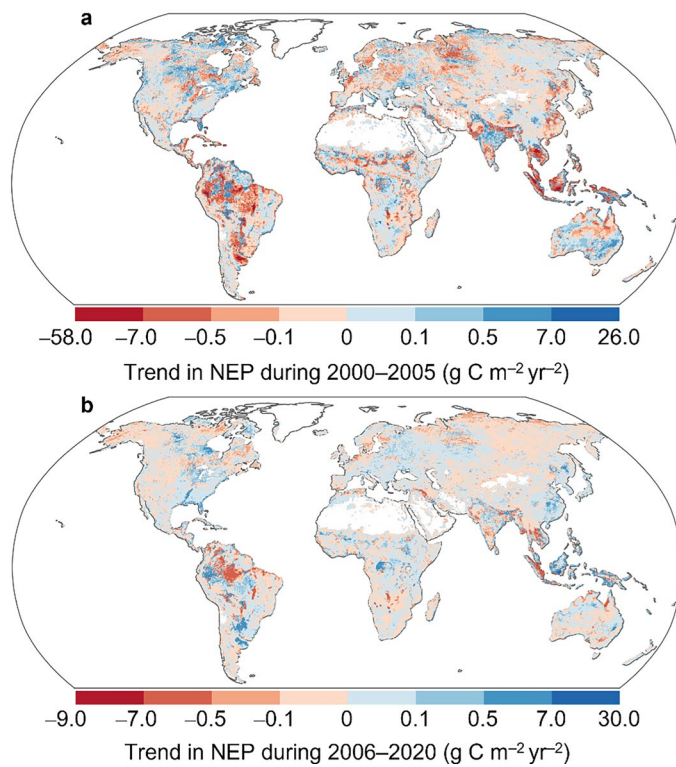
Extended Data Fig. 5 | Key factors controlling wetland water level (WL) at the global scale. Relative importance (%) of variables for predicting wetland WL identified by the random forest model. BD, soil bulk density; CTI, compound topographic index; ET, evapotranspiration; EVI, enhanced vegetation

index; fw, inundation fraction; MAP, mean annual precipitation; MAT, mean annual air temperature; NDVI, normalized difference vegetation index; PAR, photosynthetically active radiation; WTD Fan, terrestrial groundwater table depth from Fan et al.³⁶.



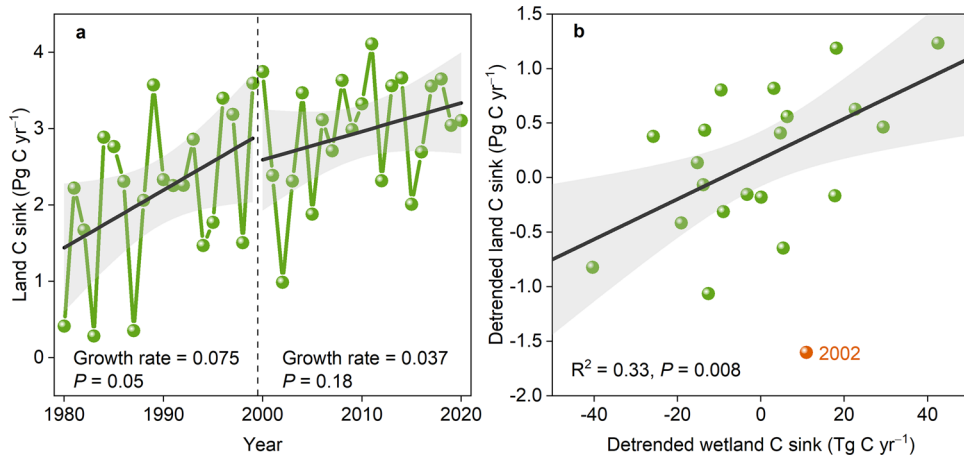
Extended Data Fig. 6 | Linear relationships of annual net ecosystem production (NEP) with mean annual air temperature (MAT) and photosynthetically active radiation (PAR) for global wetlands and wetlands in extra-tropical and tropical regions. Black solid and dashed lines represent

average predicted values and the corresponding 95% confidence interval, respectively, according to linear mixed-effect modelling. Statistical tests are conducted as two-sided.



Extended Data Fig. 7 | Temporal patterns in global wetland carbon sequestration for the period 2000–2005 and 2006–2020. **a** Global explicit map of temporal trends in annual wetland net ecosystem production (NEP) between 2000 and 2005

at $0.25^\circ \times 0.25^\circ$ resolution, which was already weighted by grid cell areas. **b** Global distribution of temporal trends in annual wetland NEP during 2006–2020 at $0.25^\circ \times 0.25^\circ$ resolution, which was already weighted by grid cell areas.



Extended Data Fig. 8 | Wetland carbon (C) sinks versus land C sinks across the globe. **a** Interannual variations in land C sinks over the period of 1980–2020. Data on land C sinks was derived from the study by Friedlingstein et al.⁶. Linear regression models were used to derive the tendency lines, which are shown as black solid lines; the error bands represent the 95% confidence interval. Statistical tests are conducted as two-sided. **b** Linear relationship between

wetland C sinks and land C sinks for the period 2000–2020. The black solid line indicates the fitted linear regression model, with the error band representing the 95% confidence interval. Statistical tests are conducted as two-sided. Data records on wetland C sinks and land C sinks are detrended at yearly time scale by removing the long-term linear trend¹⁰⁴. Land C sink in 2002 was treated as an outlier based on the Z-score outlier test, and was not included in the linear fit.

Reporting Summary

Nature Portfolio wishes to improve the reproducibility of the work that we publish. This form provides structure for consistency and transparency in reporting. For further information on Nature Portfolio policies, see our [Editorial Policies](#) and the [Editorial Policy Checklist](#).

Statistics

For all statistical analyses, confirm that the following items are present in the figure legend, table legend, main text, or Methods section.

n/a Confirmed

- The exact sample size (n) for each experimental group/condition, given as a discrete number and unit of measurement
- A statement on whether measurements were taken from distinct samples or whether the same sample was measured repeatedly
- The statistical test(s) used AND whether they are one- or two-sided
Only common tests should be described solely by name; describe more complex techniques in the Methods section.
- A description of all covariates tested
- A description of any assumptions or corrections, such as tests of normality and adjustment for multiple comparisons
- A full description of the statistical parameters including central tendency (e.g. means) or other basic estimates (e.g. regression coefficient) AND variation (e.g. standard deviation) or associated estimates of uncertainty (e.g. confidence intervals)
- For null hypothesis testing, the test statistic (e.g. F , t , r) with confidence intervals, effect sizes, degrees of freedom and P value noted
Give P values as exact values whenever suitable.
- For Bayesian analysis, information on the choice of priors and Markov chain Monte Carlo settings
- For hierarchical and complex designs, identification of the appropriate level for tests and full reporting of outcomes
- Estimates of effect sizes (e.g. Cohen's d , Pearson's r), indicating how they were calculated

Our web collection on [statistics for biologists](#) contains articles on many of the points above.

Software and code

Policy information about [availability of computer code](#)

Data collection

Data were obtained by searching for peer-reviewed articles studying wetland net ecosystem production and water level that were published before 2024 using the Web of Science, Google Scholar, and China National Knowledge Infrastructure. Full details of the search terms and filtering criteria were included in the Methods section. Detailed site-specific data such as latitude, longitude, measurement years, climate conditions, soil properties, plant variables, and elevation were also extracted from the original publications. Data presented as figures and plots were identified using Web Plot Digitizer (version 3.11).

Data analysis

Data analyses were performed using R (version 4.1.0). Packages used for analysis were: mlr3verse_0.3.1, lme4_1.1-36, randomForest_4.7-1.2, caret_7.0-1, agricolae_1.3-7. Code used to reproduce the findings of this work can be obtained at <https://doi.org/10.24433/CO.7249484.v1>.

For manuscripts utilizing custom algorithms or software that are central to the research but not yet described in published literature, software must be made available to editors and reviewers. We strongly encourage code deposition in a community repository (e.g. GitHub). See the Nature Portfolio [guidelines for submitting code & software](#) for further information.

Data

Policy information about [availability of data](#)

All manuscripts must include a [data availability statement](#). This statement should provide the following information, where applicable:

- Accession codes, unique identifiers, or web links for publicly available datasets
- A description of any restrictions on data availability
- For clinical datasets or third party data, please ensure that the statement adheres to our [policy](#)

WAD2M v.2.0 dataset can be downloaded at <https://doi.org/10.5281/zenodo.3998453>. GIEMS-MC dataset was available at <https://zenodo.org/records/13919645>. GLWD v.2.0 dataset was sourced from <https://figshare.com/s/e40017f69f41f80d50df>. FLUXNET database was publicly available at <https://fluxnet.org/data/fluxnet2015-dataset/>. MAT and MAP were obtained from https://crudata.uea.ac.uk/cru/data/hrg/cru_ts_4.05/. PAR originated from <https://doi.org/10.11888/RemoteSen.tpdC.271909>. ET was extracted from <https://doi.org/10.57760/scienceDB.10519>. Elevation was taken from <https://worldclim.org/data/worldclim21.html>. Global gridded datasets of soil properties, including SOC, pH, BD, Clay, Sand, Silt, CEC, and BS, were all collected from the SoilGRIDS database (<http://www.isric.org/explore/soilgrids>) and the Land-Atmosphere Interaction Research Group at Sun Yat-sen University (<http://globalchange.bnu.edu.cn/research/soilw>). Canopy intercept and Runoff were obtained from https://search.earthdata.nasa.gov/search?q=GLDAS_NOAH025_M_2.1. NDVI and EVI were derived from <https://earthdata.nasa.gov/>. Wetland Loss was extracted from <https://doi.org/10.5281/zenodo.7293597>. CTI can be downloaded at <https://doi.org/10.5066/F7S180ZP>. WTD Fan was obtained from <http://thredds-gfnl.usc.es/thredds/catalog/GLOBALWTDFTP/annualmeans/catalog.html>. Our compiled datasets of wetland NEP and WL can be accessed in the Figshare repository: <https://doi.org/10.6084/m9.figshare.26825293>. Source data are provided with this paper.

Research involving human participants, their data, or biological material

Policy information about studies with [human participants or human data](#). See also policy information about [sex, gender \(identity/presentation\), and sexual orientation](#) and [race, ethnicity and racism](#).

Reporting on sex and gender Not applicable. Our research does not involve human participants, their data, or biological material.

Reporting on race, ethnicity, or other socially relevant groupings Not applicable. Our research does not involve human participants, their data, or biological material.

Population characteristics Not applicable. Our research does not involve human participants, their data, or biological material.

Recruitment Not applicable. Our research does not involve human participants, their data, or biological material.

Ethics oversight Not applicable. Our research does not involve human participants, their data, or biological material.

Note that full information on the approval of the study protocol must also be provided in the manuscript.

Field-specific reporting

Please select the one below that is the best fit for your research. If you are not sure, read the appropriate sections before making your selection.

Life sciences Behavioural & social sciences Ecological, evolutionary & environmental sciences

For a reference copy of the document with all sections, see nature.com/documents/nr-reporting-summary-flat.pdf

Ecological, evolutionary & environmental sciences study design

All studies must disclose on these points even when the disclosure is negative.

Study description In this study, we first digitally mapped annual water levels (WL) in global wetlands based on 2295 field-based measurements from 606 published papers. Moreover, we constructed a worldwide dataset containing 934 in situ observations of wetland net ecosystem production (NEP) extracted from 258 peer-reviewed publications and the FLUXNET database. Finally, we modeled the spatial and temporal variations in wetland NEP using our newly established WL dataset and other environmental datasets (e.g., climate, soil, vegetation, and topography).

Research sample The global dataset of wetland net ecosystem production (NEP) included 934 site-year records collected from 258 peer-reviewed articles and the FLUXNET database, with observed years ranging from 1990 to 2023. Our compiled NEP dataset totally comprised 222 wetland sites, covering diverse climate zones and wetland types. Furthermore, we compiled 2295 site-year records of field observations of wetland water level (WL) from 606 peer-reviewed publications, with observed years ranging from 1984 to 2023. Our compiled WL dataset used in situ observations from 642 wetland sites across the globe that encompass various climate zones and wetland types. The list of peer-reviewed papers containing wetland NEP and WL data used in our study is provided in Supplementary Information.

Sampling strategy Wetland net ecosystem production (NEP) data were mainly collected by searching for peer-reviewed literature through the Web of Science, Google Scholar, and China National Knowledge Infrastructure in the period 1990-2024. The query terms for the literature search included “carbon dioxide OR CO₂ OR net ecosystem exchange OR NEE OR net ecosystem production OR NEP OR carbon OR

primary production OR respiration OR greenhouse gas OR GHG OR global warming potential OR GWP" AND "wetland OR inland wetland OR freshwater wetland OR peatland OR bog OR fen OR peat swamp OR mineral soil wetland OR marsh OR swamp OR floodplain OR tundra". We also extracted wetland NEP data from the FLUXNET database, which measures the fluxes of carbon, water, and energy between the biosphere and atmosphere based on the eddy covariance method (<https://fluxnet.org/>). Wetland water level (WL) data were obtained by searching for peer-reviewed articles that were published before 2024 using the Web of Science, Google Scholar, and China National Knowledge Infrastructure; the keywords "water level OR water table OR water depth OR groundwater OR hydrology" AND "wetland OR inland wetland OR freshwater wetland OR peatland OR bog OR fen OR peat swamp OR mineral soil wetland OR marsh OR swamp OR floodplain OR tundra" were used in the searches.

Data collection

Junjie Li, Junji Yuan, and Weixin Ding collected data. We systematically searched the peer-reviewed publications studying wetland net ecosystem production (NEP) from the Web of Science, Google Scholar, and China National Knowledge Infrastructure. To avoid bias during publication selection, the following criteria were used to screen the literature: (1) only studies using the eddy covariance method and chamber-based method were selected; (2) studies using the chamber-based method were required to have at least three replicates; (3) field observations with experimental manipulation (e.g., warming and fertilization) were excluded; (4) in situ monitoring need to have been carried out for at least one growing season (wetland sites that reported CO₂ fluxes for the growing season only were located in northern high-latitude zones; hence, we assigned non-growing season CO₂ fluxes using the estimates from Natali et al.); (5) multi-year observations within the same site were considered independent; (6) sites from open water, paddy fields, coastal wetlands, and drained wetlands were excluded; (7) floodplains that have never been inundated were excluded. The FLUXNET database includes data collected at sites from multiple regional flux networks. Of which, we identified NEP data from wetland sites and subsequently included in our global dataset. In total, our compiled database included 934 site-year records of wetland NEP observations collected from 258 peer-reviewed publications and the FLUXNET database. In addition, a comprehensive search of the scientific literature studying wetland water level (WL) was performed using the Web of Science, Google Scholar, and China National Knowledge Infrastructure. We utilized the following seven criteria to select publications: (1) the study was carried out in field conditions; (2) field observations with water-table manipulation experiments were excluded; (3) data simulated by the hydrological model were excluded; (4) the duration of the study was at least one year; (5) multi-year observations within the same site were considered independent; (6) sites from open water, paddy fields, coastal wetlands, and drained wetlands were excluded; (7) floodplains that have never been inundated were excluded. In conclusion, a total of 606 peer-reviewed publications, comprising 2295 site-year records of field measurements of wetland WL.

Timing and spatial scale

Timing scale: 2000-2020

Spatial scale: global wetlands with a spatial resolution of 0.25 by 0.25 degrees

Data exclusions

No data were excluded from the analyses.

Reproducibility

The study is fully reproducible using the data and methods detailed in the manuscript.

Randomization

Randomization is not relevant to our study.

Blinding

Blinding is not relevant to our study.

Did the study involve field work?

Yes No

Reporting for specific materials, systems and methods

We require information from authors about some types of materials, experimental systems and methods used in many studies. Here, indicate whether each material, system or method listed is relevant to your study. If you are not sure if a list item applies to your research, read the appropriate section before selecting a response.

Materials & experimental systems

- | | |
|-------------------------------------|-------------------------------|
| n/a | Involved in the study |
| <input checked="" type="checkbox"/> | Antibodies |
| <input checked="" type="checkbox"/> | Eukaryotic cell lines |
| <input checked="" type="checkbox"/> | Palaeontology and archaeology |
| <input checked="" type="checkbox"/> | Animals and other organisms |
| <input checked="" type="checkbox"/> | Clinical data |
| <input checked="" type="checkbox"/> | Dual use research of concern |
| <input checked="" type="checkbox"/> | Plants |

Methods

- | | |
|-------------------------------------|------------------------|
| n/a | Involved in the study |
| <input checked="" type="checkbox"/> | ChIP-seq |
| <input checked="" type="checkbox"/> | Flow cytometry |
| <input checked="" type="checkbox"/> | MRI-based neuroimaging |

Plants

Seed stocks

Not applicable. Our research does not involve plant material.

Novel plant genotypes

Not applicable. Our research does not involve plant material.

Authentication

Not applicable. Our research does not involve plant material.